WATER DRIVEN DEFORMATION IN SOFT SOLIDS

BY

MATTHEW PAUL MILNER

THESIS

Submitted in partial fulfillment of the requirements
for the degree of Master of Science in Mechanical Engineering
in the Graduate College of the
University of Illinois at Urbana-Champaign, 2016

Urbana, Illinois

Adviser:

Assistant Professor Shelby Hutchens

ABSTRACT

Plants have utilized water to achieve many different types of motion, using the concepts that they use, we are able to develop a self-actuated soft solid-liquid composite. This self-actuation is driven by the evaporation and resulting tension of water, which can deform soft materials. The effects that water droplets deforming in soft solids have need to be characterized in order to utilize these composites. When water is embedded in elastomeric materials, it can undergo transitions known as breathing, buckling, and creasing. Breathing and creasing have been observed. These droplets are examined in elastomers of two different elastic modulus. When droplets in the stiffer elastomer crease they form just one crease, whereas less stiff elastomers crease in multiple areas, this is the result of the surface tension. Creasing is expected to set in for any embedded droplet when it shrinks to the same relative size ratio. However, there seems to be a dependence on the stiffness, stiffer samples crease at a smaller size. The pressure in the droplets appears to not reach the expected cavitation limit, which could be a result of not taking strain hardening effects into account in calculations. After studying how a single droplet deforms in an elastomer, multiple droplets are used together in order to achieve motion resulting from evaporation.

ACKNOWLEDGMENTS

I would like to thank the Mechanical Science and Engineering Department for the opportunity to further my education and for the many resources that they make available. I would not be at this point without my undergraduate experiences at East Carolina University in both academics and athletics. The teachers, on and off the field, have developed me into the man I am today and I am extremely grateful. To my teammates and friends, thank you for giving me some much needed balance and the great memories we have had and will continue have.

Thank you to my adviser, Professor Shelby Hutchens, for having the foresight to know that we would be a good fit and giving me the chance to work with her. She has been extremely helpful in expanding my understanding of concepts and is always there to listen to and guide me when I am in need of help.

Finally, I would like to thank my family. My parents for providing me with more than I would ever need in so many aspects. My sisters for your support, I know it is tough to show it sometimes, but I hope that I have set a good example. I love y'all.

TABLE OF CONTENTS

Chapter 1: Using Water to Move Solids

Using plants as inspiration, we can develop environmentally and biologically-friendly actuation mechanisms using only water and non-toxic polymers. Plants can already achieve motion with water, so learning from what they do can lead us to effective concepts to attempt to replicate those mechanisms.

1.1. Plants Use Water for Dynamic Movements

Many plants have developed means of utilizing water to achieve motion, often using the tension in water to move surrounding material. Water plays an essential role in the life of all plants and makes up about 80-95% of the mass in growing plants. Turgor pressure, a pressure sustained within individual cells, supports the growth of plants and is important in the transportation of nutrients to all areas of the plant [1]. The absence of turgor pressure is readily observed in drooping plants that lack adequate water. In any plant, water must be pulled from the ground upwards through the stem to the leaves. This means that water must be able to withstand tensile stresses. Additionally, for droplets contained within solids, differences in humidity between the droplet and the surrounding air causes water to permeate out of the droplet and into the air. As a result, a tension is induced inside the water as it evaporates. Water has been capable of sustaining negative pressures as high as about -30 MPa in soft materials; however, when water contains dissolved solids or is in contact with surfaces, heterogeneous nucleation can reduce that pressure to values less than -1 MPa [2].

Plants in general use water to support the structure and move nutrients; however, plants also utilize water to achieve dynamic movements. These movements are often used in the reproductive life cycle to disperse seeds or spores; effective dispersal is essential to plant species

vitality. Through evolution, plants have developed various means to reproduce, exploiting their environments in the most effective ways. Whereas when a plant grows it desires adequate water to sustain itself, there are many cases where plants use the act of drying out to disperse seeds. A few plant's spore and seed dispersal mechanisms will be summarized as they relate to their use of water.

1.1.1. *Erodium cicutarium*

Erodium cicutarium is a small plant that flings seeds away from it after which the seeds bury themselves by coiling and uncoiling repeatedly in order to dig into the ground. Several awns are originally joined together in a spine, but as they dry out stresses develop and then awns are jettisoned out away from the plant. Once on the ground the process of self-burial can occur. When relative humidity is high, the awn is wet and straight, but when dried out it coils, cf. Fig. 1.1. This process drills the seed into the ground, which greatly its chances of germinating and producing a fit plant. Upon wetting a coiled awn, it unwinds about ten turns within fifteen

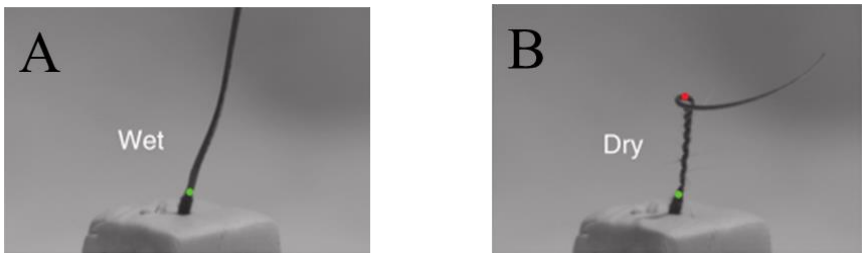

Fig. 1.1: When the awn is hydrated (A) it is straight, but upon drying (B) it coils [3].

minutes. Over the course of a few days, with repeated wetting and drying, the seed is able to completely bury itself. The cellular structure, which was likely composite, was never examined as it relates to how motion is actuated. The authors believed that regions of torsion existed in the center of the awn, while regions of bending existed outer regions [3]. Coiling of the awn takes a

relatively short amount of time, about 15 minutes; however, each species discussed hereafter is much faster, they are capable of moving in as quickly as a few milliseconds.

1.1.2. Bittercress: *Cardamine hirusta* & *Cardamine parviflora*

Both *Cardamine hirusta* and *Cardamine parviflora* utilize rapidly coiling carpels to fling seeds about a meter from the plant. A composite structure of several layers of tissue with contrasting mechanical properties is hypothesized to allow for coiling to occur. The middle and outer tissues shrink in dry environments because they are not reinforced with polymeric structural molecules, while the inner tissue remains hydrated and flexible as a result of muscillage and much thicker cells [4]. A tension is created in the outer layers when they dry out,

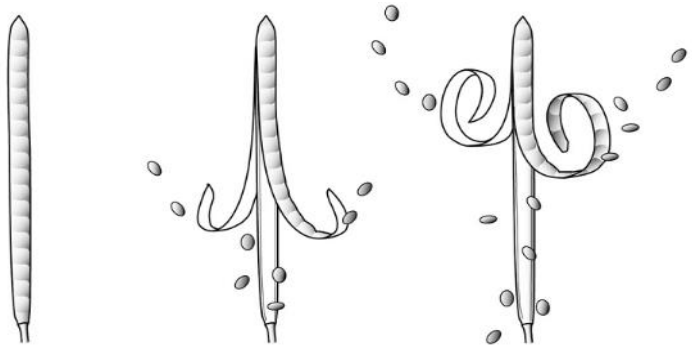

Fig. 1.2: Bittercress seed dispersal mechanism. Valves coil outward, flinging seeds out and up [20].

until enough tension has built up to break away at a weak point and coil outwards, as seen in Fig. 1.2. The energy stored in these structures is 482 μJ, and specific energy is 89.3 J/kg. The difference in tension between layers causes the carpel to coil rapidly coil outwards, in less than 5 ms. Another plant species with a similar coiling mechanism to catapult seeds is covered in the following section.

1.1.3. Jewelweed: *Impatiens glandulifera* & *Impatiens capensis*

Impatiens glandulifera and *Impatiens capensis* are made up of a seedpods consisting of five valves, which explode outwards releasing and spreading the contained seeds. The valves have a similar make up as the bittercress species. However, the bittercress curls outward, where the jewelweed curls inwards. Therefore, the layers on the inside and outside of each have opposite roles. In jewelweed, the configuration of the composite structure is such to allow an inward curl during the release of seeds. The dehydrated state of the valves is coiled, so it is necessary that an appropriate amount of turgor pressure be maintained so that the valve can remain straight while still attached to the plant. A thin membrane connecting two of the valves breaks from the force created from one valve's tendency to coil, resulting from dry environmental conditions. As the two adjacent valves begin to coil, the other connections between the valves are broken in a chain reaction causing them all to coil almost simultaneously. This synchronized movement ejects the contained seeds over the course of 2 ms [5][6].

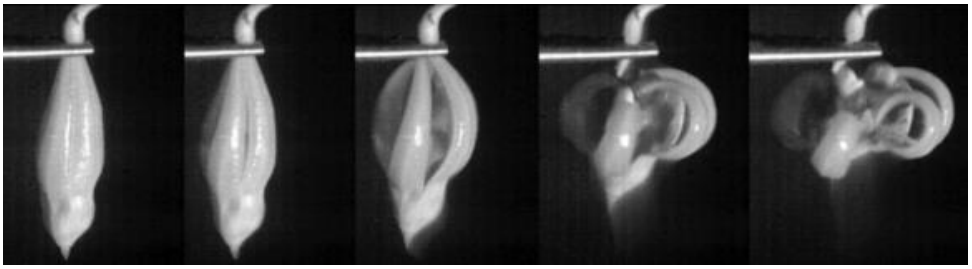

Fig. 1.3: Image sequence of an opening pod, taking place over the course of 2 ms [6].

I. capensis are *C. parviflora* both use similar mechanisms, but these mechanisms differ in how effectively they are able to disperse seeds. Upon comparing *I. capensis* to *C. parviflora*, the *I. capensis* wastes much more energy flinging seeds upwards instead of away from the plant, relatively the *C. parviflora* is five times better at flinging seeds away. This reason for this outcome is evident by comparing Figs. 1.3 and 1.4. *I. capensis* has valves that curl inwards that

tend to block seeds from escaping laterally; however, *C. parviflora* curls outwards and effectively removes any obstructions from the desired trajectory. Flinging seeds far from the parent plant is the goal in seed dispersal, especially for seeds that do not have secondary means of dispersion, like being carried by wind of being caught in an animal's fur. The benefit that *C. parviflora* receives is due to better catapult mechanics and more efficient launching, 21.3% versus 0.5%. Efficiency is defined as how well the stored elastic energy is imparted to the seeds in the form of kinetic energy. Efficiency is key, especially when the *I. capensis* has more energy available, 124 J/kg, as compared *C. parviflora* which had only 89 J/kg [5]. Curling movements in plants are achieved from a composite structure with layers of materials with mismatched properties; however, this next plant does not curl to launch pollen.

1.1.4. Bunchberry Dogwood: *Cornus Canadensis*

The flowers of *Cornus Canadensis* utilize stored elastic energy to launch pollen into the wind or onto pollinators such as bees. Unlike previously discussed mechanisms that use the

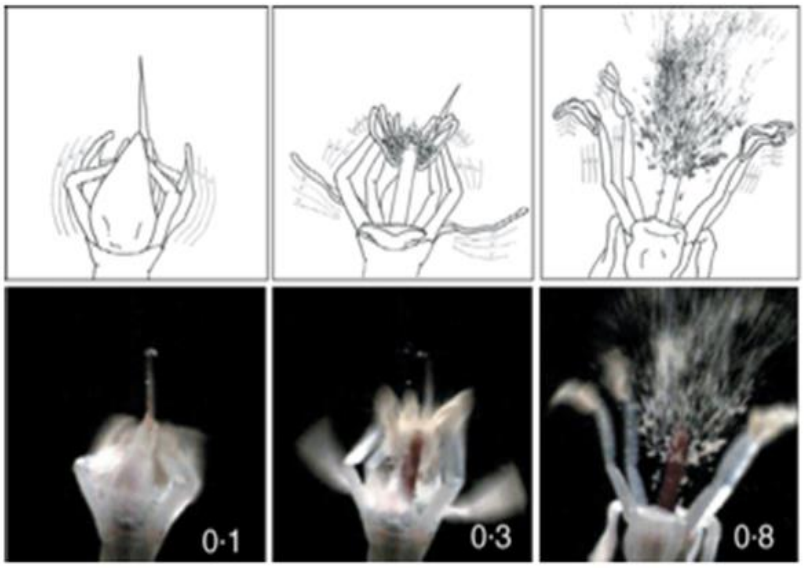

Fig. 1.4: Line drawings and image sequence of *Cornus Canadensis* pollen launching process. Images are labeled with time (ms) after opening has been initiated [7].

process of drying to launch seeds, the bunchberry uses the buildup of water, relating to increased turgor pressure, to catapult pollen. The closed petals of the flower hold down the stamens. As turgor pressure builds in the stamens, the filaments elongate until they bend over due to contacting the sealed petals of the flower. This stores elastic energy that is released when petals open. The bent filaments straighten out quickly, upon the petals opening, which catapults pollen upwards. The process of opening petals to catapult pollen occurs in under 1 ms. When the petals open naturally the pollen is released into the air and carried by wind, alternatively the petals can be opened when a pollinator of sufficient mass, a bee rather than an ant, contacts the petals which launches the pollen onto the bee [7][8]. This catapult mechanism is the fastest so far and relies solely on turgor pressure within a solid-liquid composite to achieve this speed.

1.1.5. *Polypodium aureum*

The leptosporangium is a microscopic spore catapult that uses the cavitation of water to trigger the launching mechanism. This structure is found on the dorsal side of fern fronds of the *Polypodium aureum* and similar leptosporangiate ferns. The sporangium consists of a stalk attached to an annulus. This annulus consists of a spine, with lateral walls protruding to separate about 13 cells, which is curled to enclose a cavity filled with spores, cf. Fig 1.5. Water fills each of the cells along the annulus and as water evaporates out of the cells, the tension created pulls the lateral walls of the annulus together. This effectively straightens the annulus and then curls it backwards. Evaporation creates tension within the water, but at a critical point of -9 MPa the tension causes cavitation to occur in one of the cells. Once one cell cavitates a chain reaction triggers the other cells to cavitate. This releases the annulus, flinging it forward, closing it about a third of the way, in about 10 μs. After it quickly closes, it slows down dramatically, taking a few hundred milliseconds to finish closing. The inertia imparted to the spores during the quick-

closing period carries them away from the catapult as it slows down dramatically. The reason the annulus slows is due to Darcy's Law, as strong viscous losses slow the annulus as water flows between cells [9]. The leptosporangium is an entirely self-contained mechanism similar to other mechanisms discussed; however, it is different in that it uses water to construct a liquid-solid composite. It does not utilize more than one type of solid plant material in its construction, like the curling valves in jewelweed and bittercress. Instead, it uses the properties of liquid to actuate the motion of the solid.

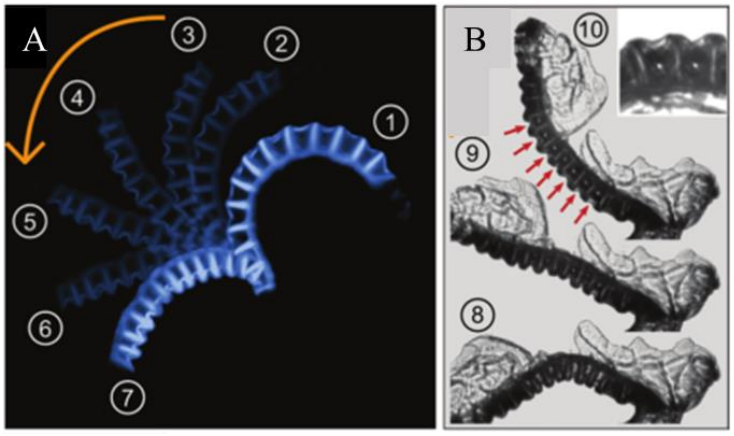

Fig. 1.5: (A) Annulus and lateral walls during sporangium opening, as water evaporates. (B) Sporangium at the point of cavitation and initiation of catapult. Three images are over 40 ms total. Red arrows show where cavitation has occurred. [9]

1.2. Two Part Make-Up of Plants

All plants that have been discussed utilize water and environmental factors to achieve dispersal of seeds or spores; however, each have evolved different mechanisms for dispersion. While all of these plants use water, there seems to be two categories that separate the plants; in one, the plants utilize solid-solid composites, whereas the other uses liquid-solid composites. The solid-solid composites employ differing mechanical properties in two or more separate layers to achieve coiling or twisting based on the cell's levels of hydration. This group includes *Erodium cicutarium, Cardamine hirusta, Cardamine parviflora, Impatiens glandulifera,* and *Impatiens capensis*. *Erodium cicutarium* uses environmental humidity levels to reversibly coil and uncoil in order to bury seeds, but the plants from the *Cardamine* and *Impatiens* genera use humidity to induce a permanent coil in the seedpod structures. This results in an explosive fracture event to launch the seeds and is irreversible. The *Cornus Canadensis* and *Polypodium aureum* fall into the liquid-solid composite group and launch pollen and spores, respectively, in an irreversible method. Furthermore, the two differ in their utilization of water in their respective processes. Whereas *C. Canadensis* requires sufficient water to build turgor pressure to arm its catapult, the sporangium relies on evaporation and eventual cavitation to launch its spores. The sporangium achieves its dynamic movement with an entirely self-contained mechanism, while the bunchberry's catapult must be held by separate anatomical structures before launching. This makes the sporangium unique due to its relatively simple makeup.

The sporangium is able to launch spores with a composite solid-liquid structure, where cellulose in cell walls is the solid portion of the composite and separates a row of compartments that hold water, the liquid portion of the composite. Water evaporates out of the compartments arching the spine until the water cavitates and flings the spine forward launching the spores. This

process is achieved entirely by environmental processes, requiring no outside forces, making it interesting as a self-actuated composite. Self-actuation allows something to be set up and then left alone; it can monitor environmental conditions and respond to those conditions when necessary. This type of mechanism would be ideal for a situation where something small and able to respond to surrounding conditions is needed, perhaps as an implantable device in the body. This opens up the question as to what types kind of deformation in soft materials can be caused by the internal tension of water caused by evaporation. This idea motivates the following research.

Chapter 2: Materials and Methodology

The following sections will cover the selection of a material for the matrix, the production of samples, and the process of observing droplets of water within a soft matrix. The material must be soft and able to be embedded with water droplets in a way that the samples can be considered analogous to leptosporangiate ferns. This will enable results obtained from samples to be analogized to what occurs in those plants and how that can be mimicked.

2.1. Material Selection

As water evaporates within a solid structure it is in a state of tension, this tension would be expected to deform the surrounding solid if it is compliant enough, as in a plant. Polydimethylsiloxane (PDMS) is a soft, elastic material similar to rubber and is optically clear. Sylgard 184, from Dow Corning, is a two-part kit used to make PDMS. The mixing ratio of pre-polymer to curing agent can be changed to vary the degree of polymerization and the final stiffness of the PDMS. Furthermore, as PDMS is optically clear, water droplets within it are visible.

2.2. Sample Preparation

Samples are created from liquid PDMS and must be molded into reproducible configurations so that a systematic process can be used to study embedded water droplets. The mold must be precise and made of multiple pieces, thus being able to be separated, in order to release the sample without damaging it. Additionally, it must be able to withstand the temperature required to cure the PDMS, in about an hour. Acrylonitrile butadiene styrene (ABS) a thermoplastic polymer has a glass transition temperature of 105° C and can be 3D printed easily. The glass transition temperature is high enough that PDMS can be cured at 80° C without

destroying the mold. A diagram of the mold is shown in Fig. 2.2; note that the shape of the resulting PDMS sample will be a rectangular prism. Multiple samples are made at the same time, which allows for a greater chance of creating a usable sample, where the embedded water droplet remains in the center of the sample while curing. PDMS is a viscous fluid before curing and has a specific gravity of 1.03. Furthermore, PDMS is hydrophobic and immiscible with water. These factors cause embedded water droplets within uncured PDMS to tend to rise to the top during curing. In order to keep water droplets in the middle of the PDMS sample, it can either rotate during curing or cure at sufficiently high temperature so that the PDMS solidifies before the droplet rises to the top. A stepper motor attaches to the mold via a hub to spin the mold during curing.

The following is the procedure used to create PDMS ready for curing:

1. Weigh out about 40 g of PDMS base polymer
2. Divide the weight of base polymer by 10 or 25, depending on whether a 10:1 or 25:1 mixing ratio is used, respectively
3. Add the calculated weight of crosslinking solution from number 2 and mix vigorously for about 2 minutes
4. De-gas the mixture for about 45 minutes, or until all air bubbles in the mixture are gone

Before pouring the PDMS into the mold, insert polymethylmethacrylate (PMMA) slides into the mold. PMMA and PDMS will not bond and as the PDMS cures against the PMMA, it creates a flat surface that is optimal for viewing internal voids. After clipping the three pieces of the mold together, PDMS is slowly poured down the side of the mold to avoid creating bubbles. After the molds are filled carefully, pipette 10 µL of de-ionized water into the center of the mold. After embedding droplets, one of two methods can be used to cure the PDMS. The first method uses spinning the mold while in the oven. The open top of the mold is sealed with a strip of previously cured PDMS, held down with rubber bands. The mold is connected to the stepper motor and placed into the oven that is set at 80° C. The stepper motor rotates the mold at 5 rpm. The sample remains in the oven for one hour and then samples are removed from the mold. The second method uses a higher temperature and anticipates that the droplets will rise. Instead of spinning the mold in the oven, the water droplets are inserted lower into the PDMS and the temperature of the oven is increased to 90° C. This reduces the required curing time, about 45 minutes. The water droplets still rise during curing, but the PDMS stiffens quickly enough to set

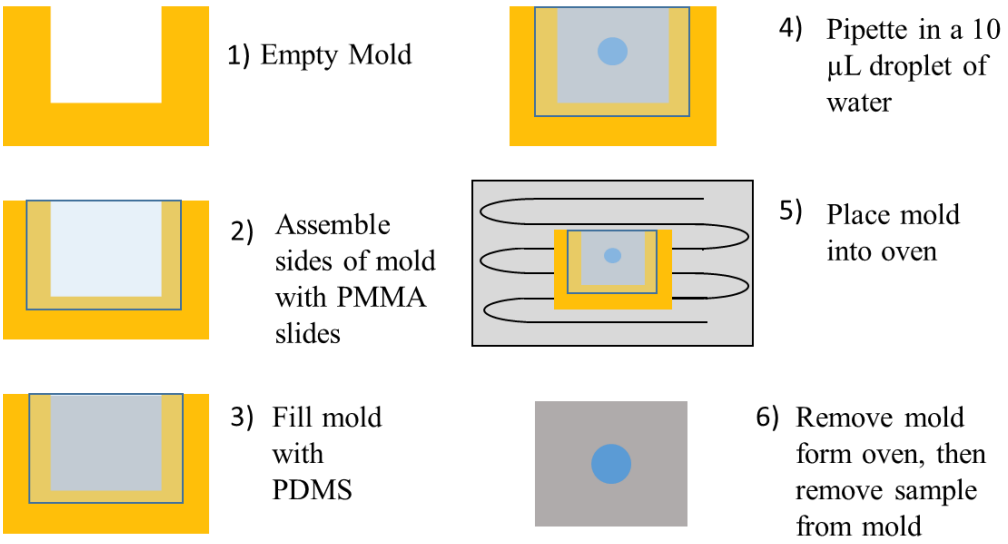

Fig. 2.1: Steps taken during the process of sample preparation

them in the middle of the sample. The overall process of sample preparation is summarized in Fig. 2.1.

2.2.1. Mold Geometries

Three different shapes of molds are used. One has a rectangular cross section, where the length and the width of the cross section is 25 mm and 7 mm, respectively. The other two molds have square cross sections, where one was thick and the other was thin. In the thin molds, the cross section is 7 mm by 7 mm; meanwhile, in the thick mold the cross section is 22.5 mm by 22.5 mm. The 7 mm dimension was determined to be sufficiently thin, because a 10 μL droplet

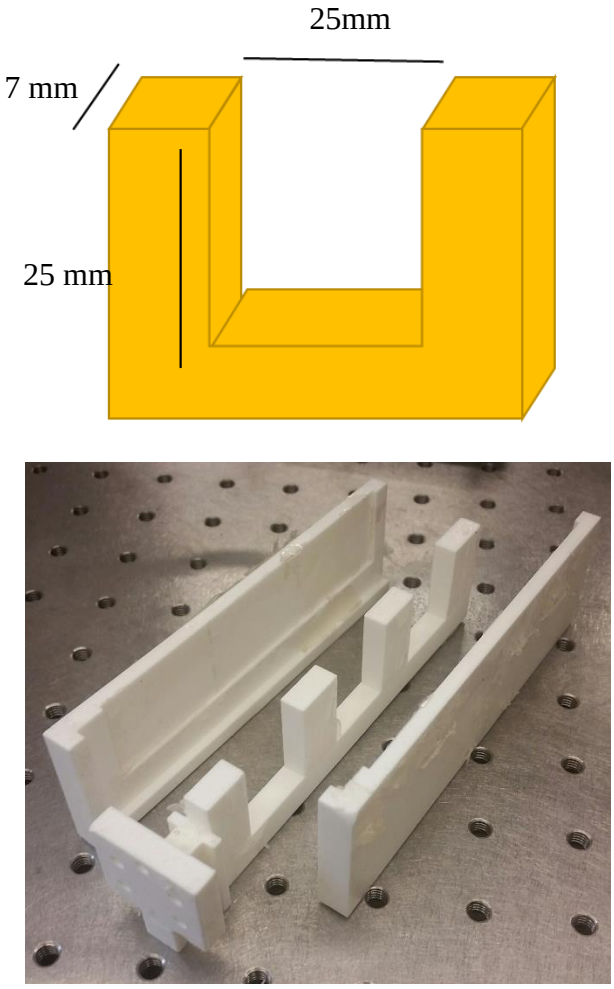

Fig. 2.2: Schematic showing dimensions of mold geometry (top) and an image of the actual mold (bottom).

has a diameter of 2.68 mm, which means that if the droplet is in the center of the mold, then it is within one diameter of each boundary. Alternatively, in the thick cross section, a droplet placed in the middle will be about four droplet diameters from the boundary, far enough to be considered substantially different from the thin. The square cross section molds had PMMA slides surrounding the cavity, so that four sides of the eventual sample were prepared for viewing. The finished samples are shown in Fig. 2.3 and the molds that created them are shown in Fig. 2.4.

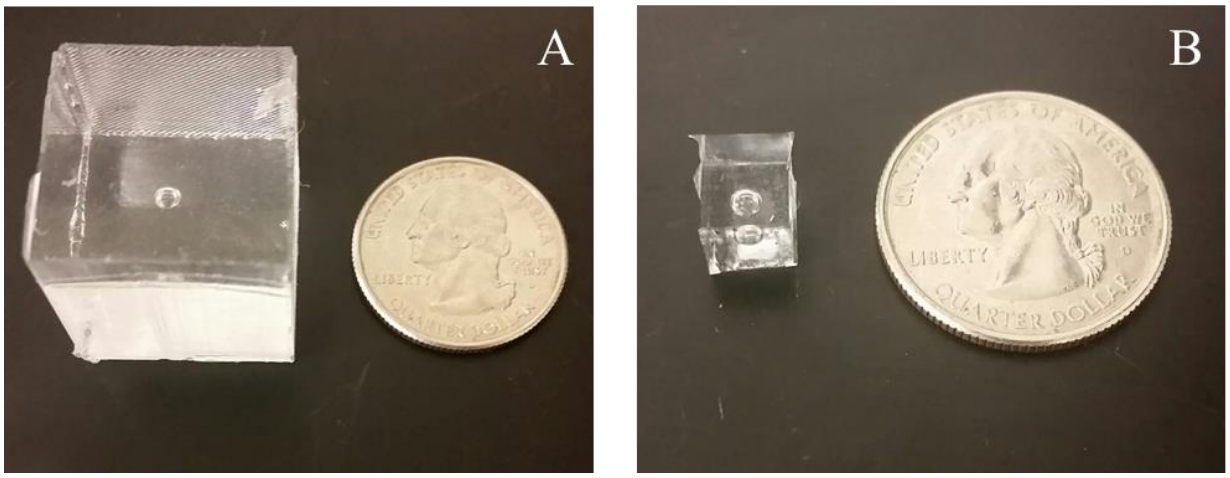

Fig. 2.3: Typical samples of thick (A) and thin (B) geometries, with a U.S. quarter for scale.

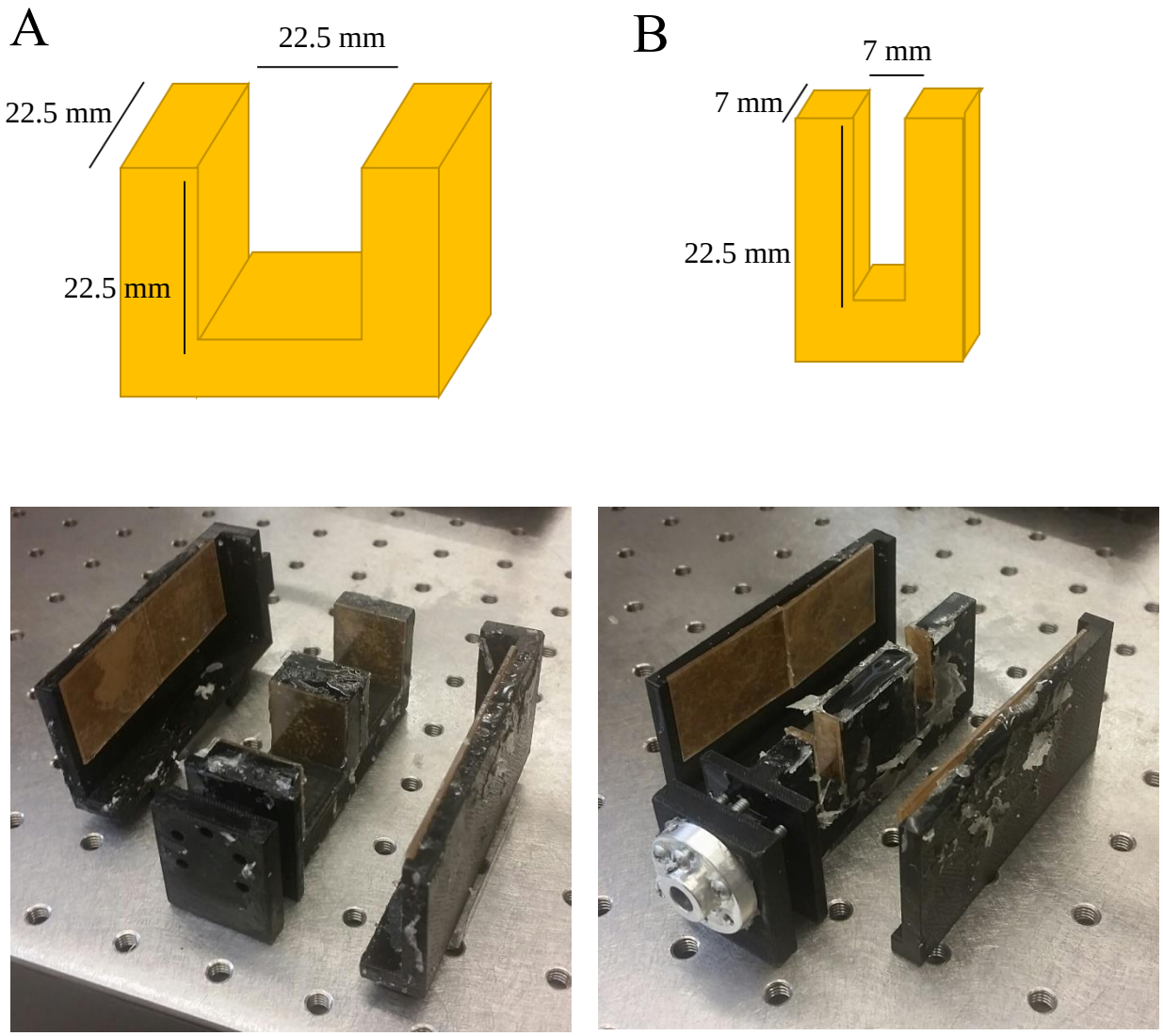

Fig. 2.4: Schematics showing dimensions of mold geometry (top) for thick (A) and thin (B) samples. Images of the actual molds for each geometry (bottom). The brown areas are PMMA slides with paper backing still on them.

2.3. Droplet Observation

Observations occur while the embedded water droplets dry and images are taken to record the droplets throughout the process. A lightbox diffuser housed each sample while LED lights backlit the sample, in order to provide uniform lighting conditions throughout the course of observation. Within the lightbox, a small resistive heater served as the platform to hold the samples. The heater expedited droplet evaporation; without it, droplets took a few weeks to cavitate, but with it, this time decreased to a few days. A CCD camera captured images of the droplets every fifteen minutes, for the duration of droplet evaporation, which was typically a few days. Samples with a square cross section require additional steps in order to see the droplets from two different sides. These samples were rotated 90° every fifteen minutes by means of a stepper motor attached underneath the platform that held the samples. The focal distance of the sample tended to change upon rotation, necessitating that the camera move into focus. Therefore, an actuated linear stage moved it to the correct distance to focus the droplet. Each fifteen minutes

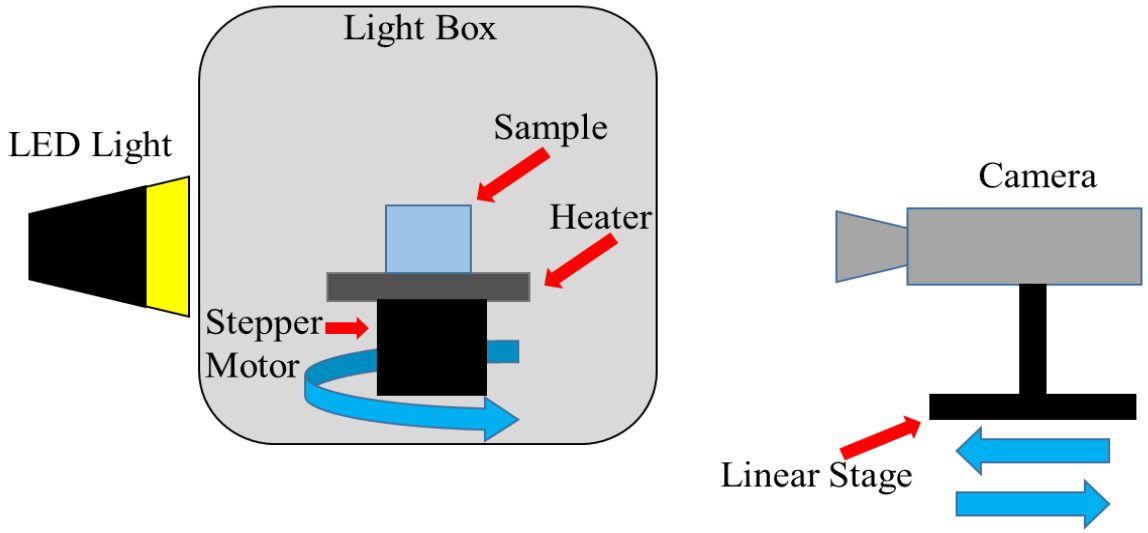

Fig. 2.5: Schematic showing experimental set up for droplet observation. An LED light illuminates the area of the light box, behind the sample. The sample is on top of a heater, which is able to rotate back and forth due to a stepper motor. A camera slides back and forth to keep the droplet in focus, after the sample rotates.

the sample would rotate and the camera would move to take pictures of alternating sides. Above is the setup for droplet observation.

2.4 Soft Solid-Liquid Composite Actuator

A self-actuatable soft solid-liquid composite that mimics the behavior of the leptosporanguim spore launching mechanism was created using similar techniques that created the various types of samples studied. The ultimate goal was to place multiple water droplets in a line, embedded within a soft-solid matrix. This is the same general concept as creating the previously mentioned samples, except that multiple droplets of water are used. Although the actual leptosporangium is curved, the replica is created in a straight configuration to demonstrate capabilities while keeping the fabrication simple. The mold that is used is shown in Fig. 2.6. The mold consists of three pieces to allow the cured replica to be easily removed, but no top piece is used. When the top was sealed it tended to move the droplets around because it forced the viscous PDMS to be moved around, distorting the droplets. Leaving the top off the mold kept the droplets in their original places and spherical; however, now the mold cannot be spun in the oven without everything leaking. In order to combat the rising of the droplets during curing, the

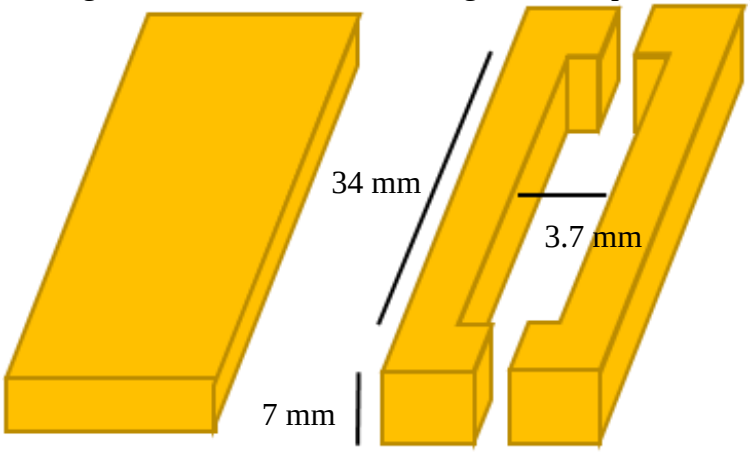

Fig. 2.6: Schematic of a three-piece mold used to create replicas. The piece on the left is the bottom of the mold, and the pieces on the right get PDMS poured into the center.

droplets are placed low in the mold and the temperature of the oven is set at 95°C. This cures the PDMS quickly enough so that the droplets are trapped in the middle of the mold. Then excess PDMS can be trimmed after curing to establish desired boundary conditions. A mixing ratio of 25:1 was used to create the replicas.

During fabrication of samples, typically about 13 droplets of water are inserted into the PDMS with minimal spacing, about one droplet radius, in between them. Using a pipette with a wide plastic tip is quite obtrusive when inserting multiple droplets. It must be removed from the PDMS after each droplet is placed and the tip must be changed since it becomes clogged with PDMS. A better alternative was to use a syringe with a thin metal tip. A syringe can hold plenty of water and can precisely place droplets, without the need to withdraw it from the PDMS between droplets. The downside to this method is that the precision of uniform droplets is lost; however, the fern leptosporangium does not use uniform compartments sizes.

Replicas are set up over the resistive heater and observed in the same manner as previously mentioned for samples; this set up is shown in Fig. 2.7. The finished replica is shown in Fig. 2.8.

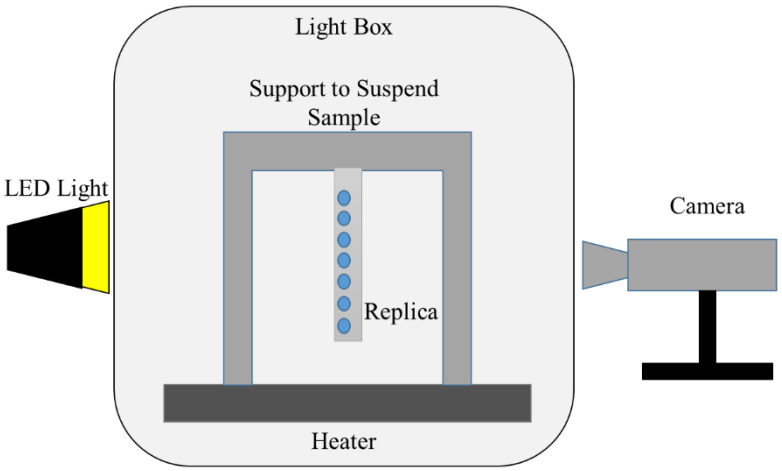

Fig. 2.7: Schematic showing experimental set up for replica observation. An LED light illuminates the area of the light box behind the sample. The replica is suspended over the heater.

Fig. 2.8: A finished leptosporangium replica, after the water has evaporated from the droplets. A U.S. quarter is used for scale.

Chapter 3: Results and Analysis: Droplet Deformation

A main goal of this project was to study what happened to elastomeric soft solids as embedded water droplets deformed the elastomer, during the process of evaporation. Knowledge gained from this study was used to aid in the design and replication of leptosporangium-like actuators.

3.1. Tracking Droplets During Deformation

This study tracks droplets, by measuring their radii, while water evaporates from them up to the point of cavitation. Images of the droplet are taken at fifteen-minute intervals. ImageJ, an image analysis software, analyzes the images. It sets thresholds to isolate the darker droplets from the lighter background and then automatically calculates the area of the droplets, from which a radius of the droplet can be determined.

3.2. Expected Trends: Breathing-Buckling-Creasing-Cavitation

Theory predicts that droplets can undergo transitions known as "breathing," "buckling," and "creasing;" depending on strain and boundary conditions as spherical droplets of water

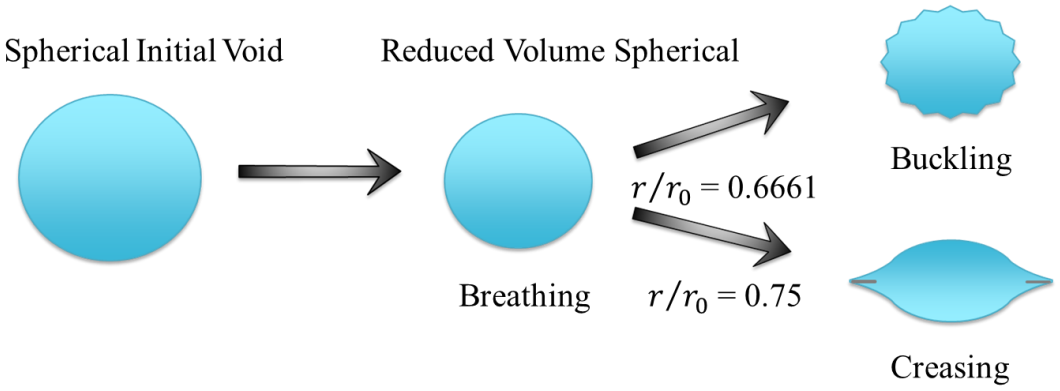

Fig. 3.1: A spherical droplet of water will begin deforming by breathing, and then it can either buckle or crease, depending on strain conditions.

shrink while within an elastomer. The first step in this process is breathing, where a droplet reduces in size, while remaining spherical, as water evaporates. As the droplet continues to deform it will take on either a buckled or a creased configuration, depending on which configuration minimizes the free energy depending on strain conditions. Creasing for spherical droplets is expected at a stretch ratio of 0.75, when strain is finite, while buckling is expected at a stretch ratio of 0.6661, when strain is infinitesimal [10]. Figure 3.1 summarizes this process.

3.2.1. Criterion for Breathing, Buckling, and Creasing

The possible stages that droplets deforming in elastomers can go through include breathing, buckling, and creasing. Once a droplet of water is inside of an elastomer, the water will begin to evaporate. Differences in humidity inside and outside the droplet give rise to a difference in chemical potential and is the driving force for evaporation and the resulting droplet deformation. The water is under tension as it evaporates and that tension can deform surrounding elastomers. The first stage of deformation, as the droplets dry out, is denoted as breathing. This is essentially a shrinking of the droplet, while maintaining spherical geometry. After this stage, if a "small deviation" occurs then the droplet takes on either a buckled or a creased configuration. Buckling occurs when, "deviating from breathing by a field of strain that is infinitesimal in amplitude, but finite in space"; meanwhile, creasing occurs when, "deformation deviates from breathing by a field of strain large in amplitude, but infinitesimal in space." [10] A stretch ratio, r/r_0, is defined for the droplet, where r is the length of the deformed radius and r_0 is the length of the undeformed radius. Given the aforementioned strain conditions, buckling is predicted to set in, after breathing, when the stretch ratio reaches 0.6661. Alternatively, in the strain conditions for creasing, creasing should be expected when the stretch ratio is 0.75. The reason that the droplets will take on these configurations is due to the minimization of the free energy of

the system. The free energy consists of the elastic energy of the elastomer and the potential energy due to the internal tension of the system. Note that as the droplet shrinks, the criteria for creasing are met first, thus buckling, which involves a concerted, global deformation of the surface, has not been predicted due to the primary occurrence of localized creasing [10].

3.2.2. Droplets Crease but Never Buckle

Six different types of samples were tested, this included three varying thicknesses of samples, of which, both 10:1 PDMS (stiffer) or 25:1 PDMS (softer) are used. The tabulated results for which type of sample reached each type of configuration is shown in Table 3.1.

Sample Type	Breathing	Creasing	Buckling	Cavitation
10:1 Thin	5	5	0	5
10:1 Asymmetric	5	5	0	5
10:1 Thick	5	3	0	5
25:1 Thin	5	5	0	5
25:1 Asymmetric	5	5	0	5
25:1 Thick	5	4	0	5

Table 3.1: Number of droplets that were observed in each configuration. For each sample type, five droplets were observed.

All droplets underwent breathing, then most crease, and then all cavitate; however, no droplets buckle. A possible reason as to why they fail to buckle could be from the boundary conditions as the onset of buckling was not considered for a spherical void in a finite elastomer [10]. Furthermore, the theory was developed by assuming that a *spherical* droplet was embedded in the center of a *spherical* elastomer. In the experimental setup, the samples had *spherical* droplets embedded in *cubic* elastomers. This causes the thickness of the boundary to vary may prevent the droplet from achieving the homogenous strain at the surface necessary for buckling.

3.2.3. Droplet Deformation Over Time

Thirty droplets were observed over the course of this study, three representatives droplets are shown in Fig.3.2, which shows the stretch ratio of the droplet over time. One of these droplets cavitates during breathing, but the other two cavitate after creasing. Images of droplets at indicated points are shown in subsequent figures. The 10:1 representative sample has only one crease that channels around the droplet during creasing. This trend is observed in all 10:1 or stiffer samples. Alternatively, in the 25:1 softer sample, multiple creases form.

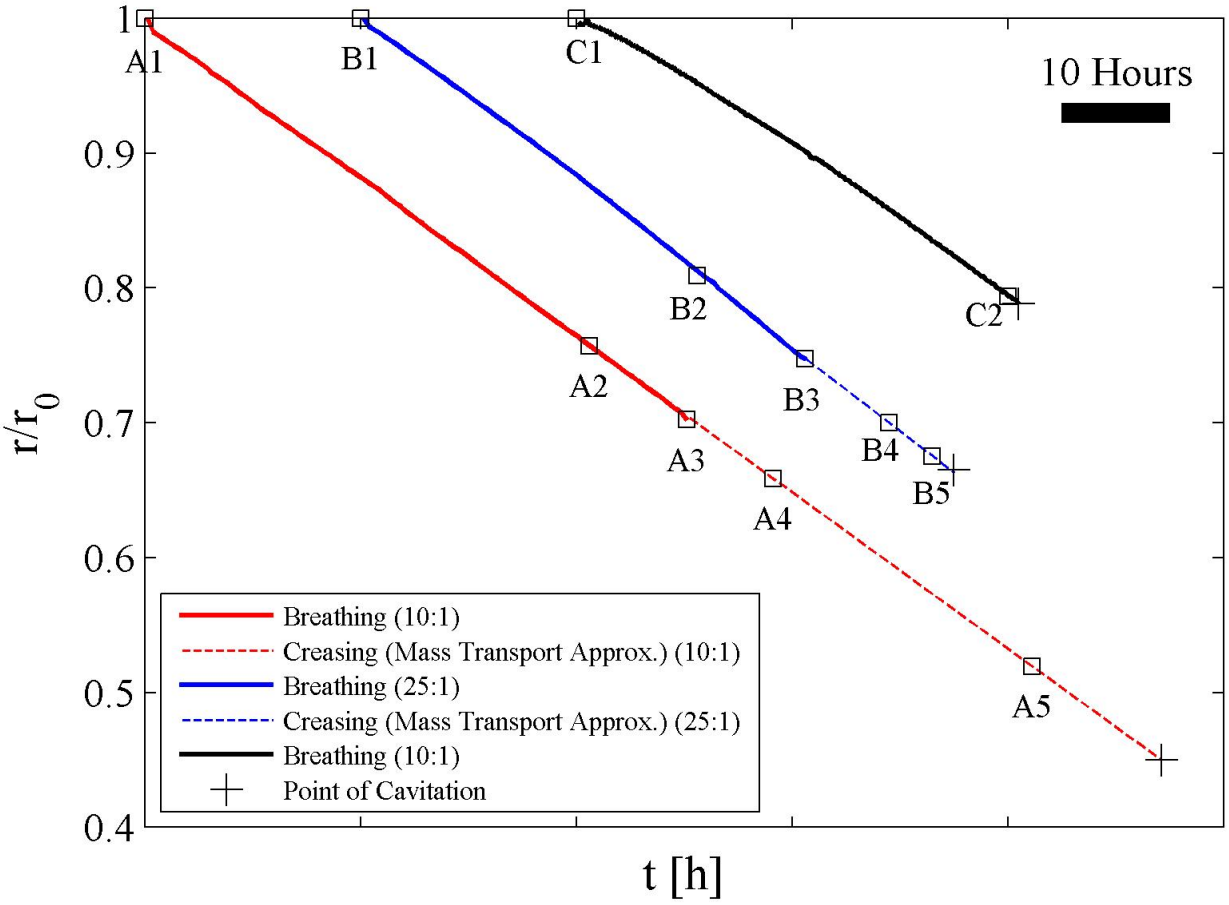

Fig. 3.2: Representative curves of droplet deformation. The curves labeled with points "A," "B," and "C" show 10:1, 25:1, and 10:1 samples, respectively. Solid lines connect actual data points, where dashed lines are approximations of creasing up until the time that cavitation occured. The red and blue curves crease and then cavitate, but the black curve never creases.

The red curve, c.f Fig. 3.2, denoted with points “A,” is a 10:1 sample that creases in one spot and then channels around the droplet. Fig. 3.3 shows the droplet as it deforms, with the points in Fig. 3.2 corresponding to the images labeled in Fig. 3.3.

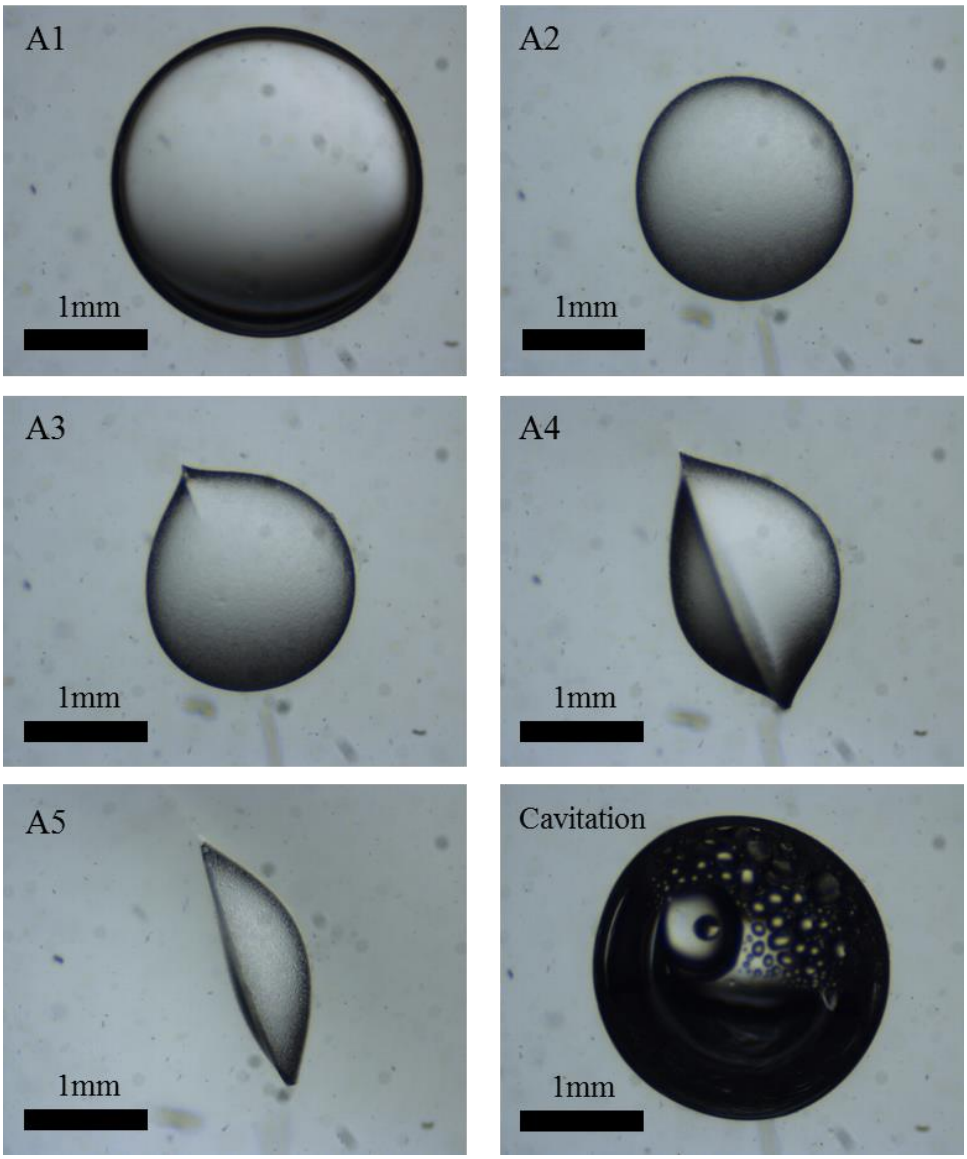

Fig. 3.3: Images from the points indicated in Fig. 3.2 from the red curve, with points “A.” (A1): Initial droplet. (A2): Droplet in breathing region. (A3): A single crease sets in. (A4): The droplet continues to deform along the single crease. (A5): Droplet has deformed extensively and then cavitates (Cavitation).

The blue curve, c.f Fig. 3.2, denoted with points “B,” is a 25:1 sample that creases in many areas of the droplet. Fig. 3.4 shows the droplet as it deforms, with the points in Fig. 3.2 corresponding to the images labeled in Fig. 3.4.

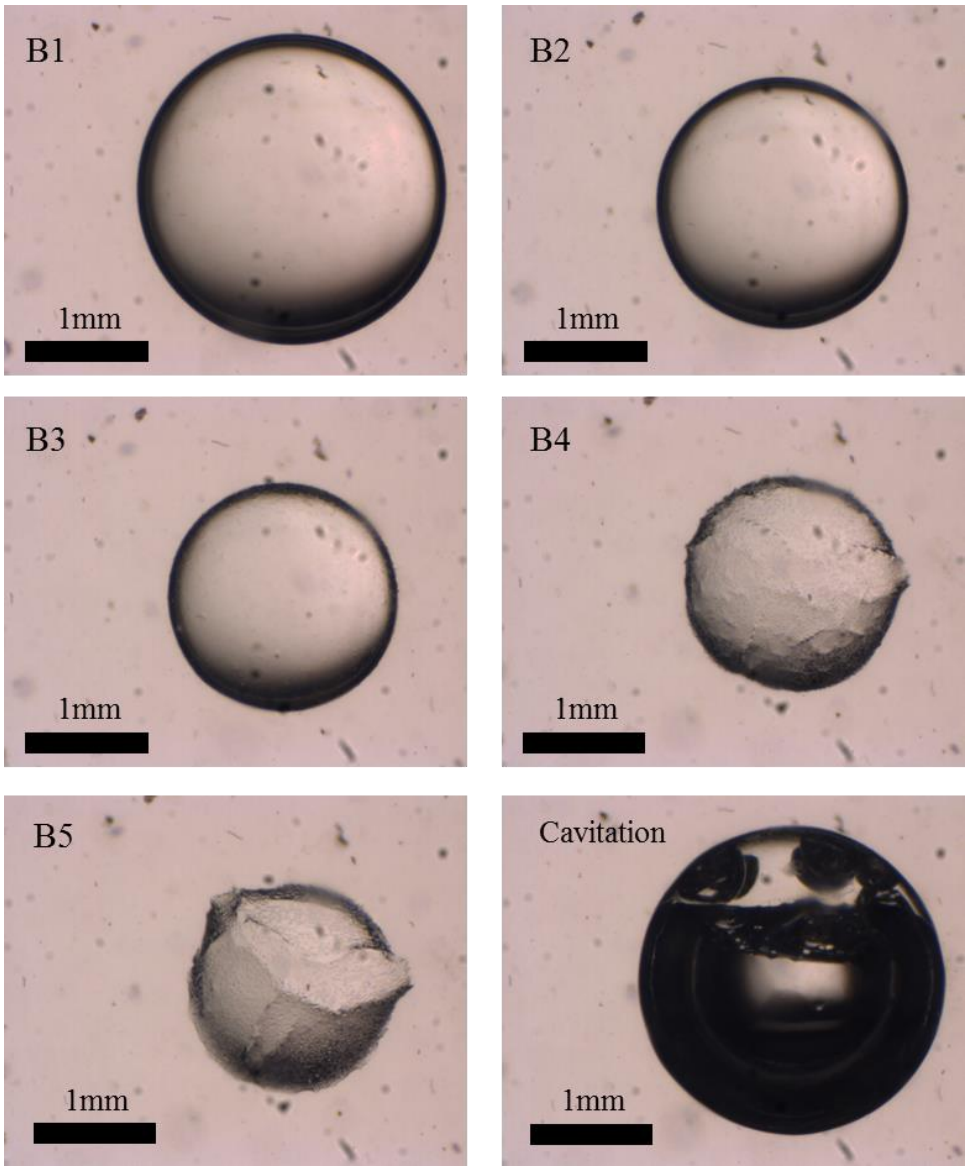

Fig. 3.4: Images from the points indicated in Fig. 3.2 from the blue curve, with points “B.” (B1): Initial droplet. (B2): Droplet in breathing region. (B3): Point at which multiple small creases are first observed. (B4) and (B5): Creases grow form the initial areas observed in (B3), until cavitation occurs (Cavitation).

The black curve, c.f Fig. 3.2, denoted with points “C,” is a 10:1 sample that cavitates before any creases form. Fig. 3.5 shows the droplet as it deforms, with the points in Fig. 3.2 corresponding to the images labeled in Fig. 3.5.

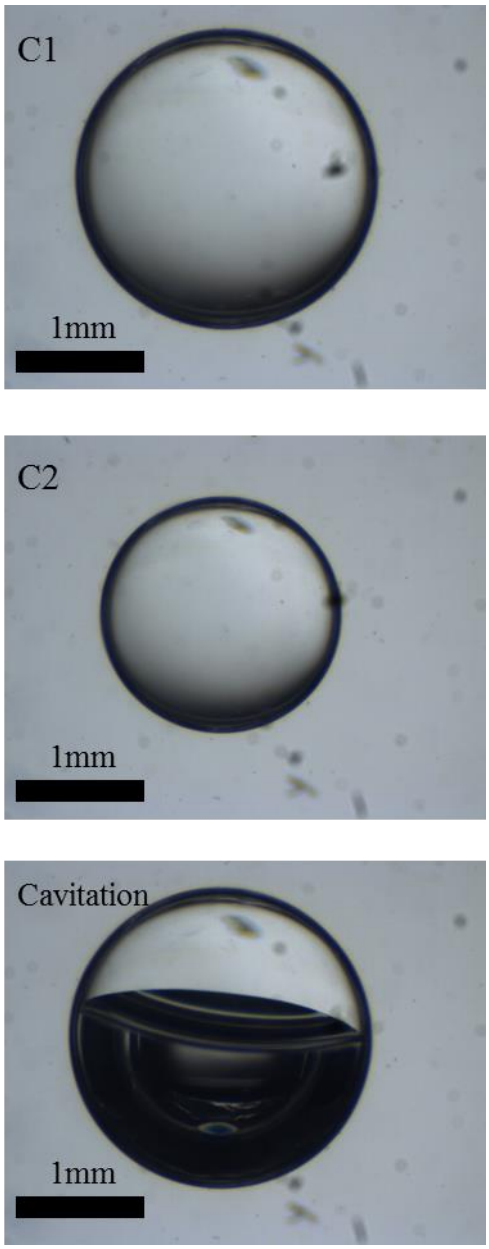

Fig. 3.5: Images from the points indicated in Fig. 3.2 from the black curve, with points “C.” (C1): Initial droplet. (C2): Droplet in breathing region. (Cavitation): Droplet cavitates before creasing.

Table 3.2, below, summarizes the number of creases that the droplets have (when creasing is observed) just prior to cavitation. In each 10:1 sample, regardless of thickness, only one crease forms, except in one instance where four creases formed. However, this is quite different from what occurs in the softer, 25:1 samples. In these samples, a large number of creases form in many areas of the droplet. The stiffer samples generally have creases confined to one area of the droplet. None of the asymmetric samples are included in this table because they were only observed from one direction and therefore the number of creases could not be accurately determined.

	Number of Creases				
Sample Type	Sample 1	Sample 2	Sample 3	Sample 4	Sample 5
10:1 Thin	1	1	1	1	1
10:1 Thick	1	No Creasing	No Creasing	1	4
25:1 Thin	Multiple	Multiple	Multiple	Multiple	Multiple
25:1 Thick	No Creasing	Multiple	Multiple	Multiple	Multiple

Table 3.2: The number of creases formed for each of the five samples, within each sample type. “Multiple” creases refers to a numerous amount of creases that seem to form all over the droplet concurrently. This only occurs in softer samples. A small number of creases, i.e., 1 or 4, appear in stiffer samples.

Stiff, 10:1, samples have creases that nucleate once and then channel around the droplet, while less stiff, 25:1, samples nucleate in multiple spots and then all continue to channel. Experiments have shown that nucleation and channeling of creases can be hampered due to surface energy [11]. An elastocapillary number, $\gamma/(\mu\, r_0)$, was used to study nucleation and channeling of creases. The surface energy is, γ, shear modulus is, μ, and r_0 is the length of a

droplet. The surface energy, γ, of PDMS on water is 40 mN/m [11]. For 10:1 PDMS, Young's Modulus is about 2.6 MPa while for 25:1 PDMS Young's Modulus is about 1 MPa [12]. The shear modulus, μ, of each is 0.867 MPa and 0.333 MPa, for 10:1 and 25:1 PDMS respectively. Since droplets are all roughly the same size, with a radius of 1.32 mm, the length scale is consistent for all samples, The shear modulus is the only difference between samples, resulting in the 10:1 samples having a lower elastocapillary number, $\gamma/(\mu\, r_0)$, than the 25:1 samples, based on μ alone. A lower value of $\gamma/(\mu\, r_0)$ has been shown to enable creases to channel further [11]. This is in agreement with what is observed in the 10:1 relative to the 25:1 samples. Since the 10:1 samples crease in one spot and then that crease is able to readily channel around the droplet. Although a lower value of, $\gamma/(\mu\, r_0)$, aligns with what was observed with regard to channeling, it is expected to cause creases to set in at lower levels of strain, but this is not what is observed in the onset of creasing.

3.3. The Onset of Creasing

All droplets that deviated from breathing did so by creasing. Creasing was expected to take place at a value of $r/r_0 = 0.75$. This prediction holds if the sample was made of 25:1 PDMS; however, if the sample is made of 10:1 PDMS creasing occurs past this point. These results are shown in Fig. 3.6.

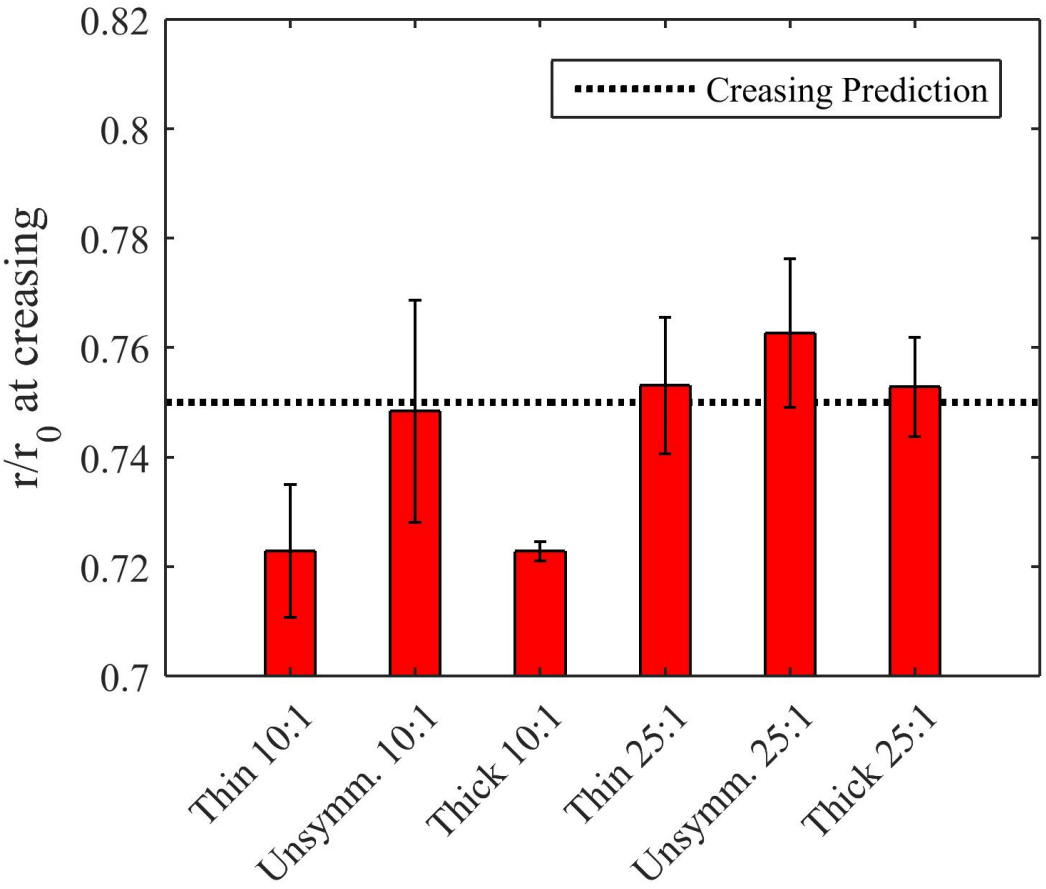

Fig. 3.6: Value of r/r_0 at the point that creases are identified. Stiffer samples crease below the expected value of 0.75, while less stiff samples crease above this value.

Asymmetric samples of 10:1 and 25:1 PDMS differ from the results of their respective thin and thick counterparts. These samples were the first to be tested and most likely were susceptible to systematic error that increased the value of the measured crease ratio. This could potentially be from measuring these droplets with the automatic threshold set by ImageJ, while in latter samples the threshold was adjusted manually for the best fit. Automatic thresholds did not always match up to the edge of the droplet. In addition, the thresholds that were used did not seem to match up exactly before and after processing. Regardless of this potential error between asymmetric and symmetric samples, there is still a clear deviation from the expected value of

creasing and trends have developed. The average ratio for 10:1 samples at creasing is 0.731, while for the 25:1 samples it is 0.756. The droplets embedded in stiffer PDMS crease at a higher stretch ratio than those droplets in less stiff PDMS. Surface energy, and the elastocapillary number, $\gamma/(\mu\, r_0)$, are expected to cause 25:1 samples to crease at a higher stretch ratio than 10:1 samples [11]. The opposite trend is observed. This could be related to droplets being on a length scale much larger than the elastocapillary length. Elastocapillary length is defined as γ/μ and has effects for length scales of similar order [13]. The elastocapillary length will play a larger role in the 25:1 PDMS, but even this length is 1.2×10^{-7}m, which is still 10,000 times smaller than the radius of the droplets. In the previous section (3.2.3.), the effect of surface tension was confirmed with other experiments for the role it has in channeling [11]. This could be a coincidence, since this term should be miniscule at these scales. It appears that in the onset of crease formation that another phenomenon has dominated the effect of surface tension. This could be due to the effect of the stiffness of the material. The onset of creasing has been observed to vary slightly in sheets of hydrogels. The hydrogels ranged in shear modulus from 0.6-24 kPa and creased at strains of 0.33 ± 0.02. The stiffer the hydrogel, the higher the strain for creasing [14]. This corresponds to the same phenomenon seen in the 10:1 and 25:1 samples. These samples had a much higher shear modulus than the hydrogels, but the trends should still hold as they relate to the onset of creasing.

3.4. Rates of Deformation

Water leaves the droplet due to a difference in humidity inside and outside of the droplet, permeating through the elastomer and then evaporating into the surrounding air. The rate of droplet deformation is shown in Fig. 3.7.

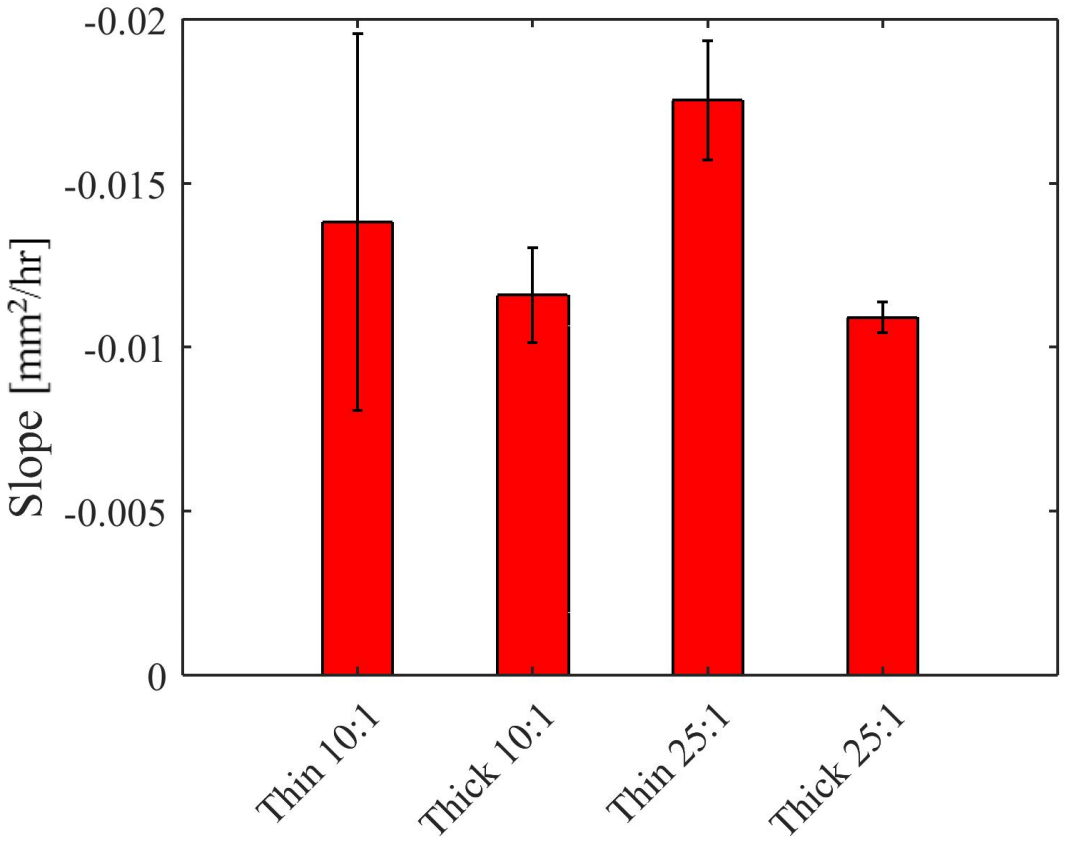

Fig. 3.7: Thin samples shrink at a faster rate than thick samples, regardless of stiffness of samples. This is caused by a higher magnitude of heat being able to reach the water droplet.

There is a dependence on the rate of evaporation based on the boundary thickness; thinner samples tend to evaporate more quickly than thicker samples. More heat can be applied to the droplets in the thin samples, whereas the thick samples are more insulated. Only the thick and thin samples are shown because the asymmetric sample data did not contain enough points to determine an accurate slope measurement. The rate of deformation is also based on the

magnitude of the temperature at the droplet location. The distance from the bottom of the sample to the droplet varied within all samples and heat was applied only at the bottom of the samples. Droplets that are slightly higher from the heat source were cooler and therefore experienced a slower rate of evaporation. The wider variation in the 10:1 thin samples is due to droplets at different heights relative to the heater. This set of samples was the first that were observed of all samples and once techniques for droplet placement were perfected, the scatter in the data was reduced.

Evaporation is the driving force in droplet deformation and a linear relationship exists between the radius squared and time. Assume there is a sphere of water with radius, r, over time the water will evaporate and the radius of the droplet will decrease.

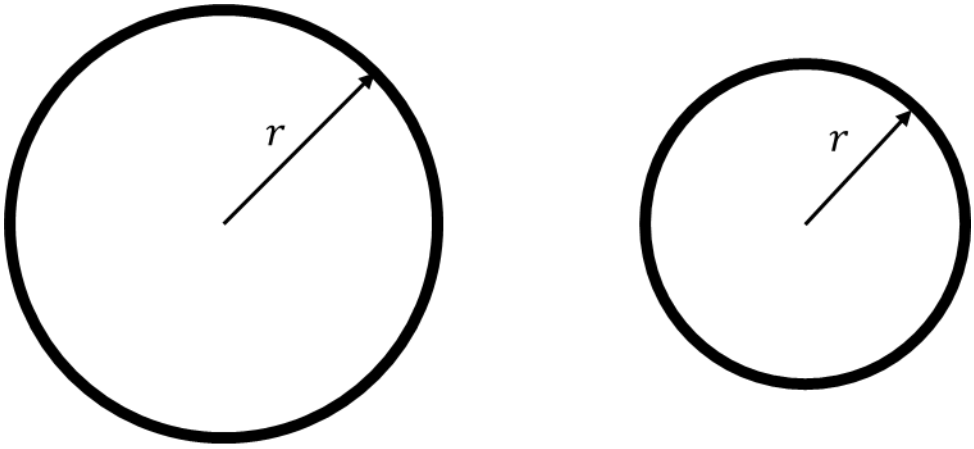

Fig. 3.8: At time $T = 0$ the radius of the droplet is at its initial size, $r = r_0$. At a later time $T > 0$ the radius has decreased, $r < r_0$.

We will start with the rate of mass transfer and show a derivation relating the radius and time [15]. The molar flux of water vapor (A) into air (B) is given by.

$$N_{A,r} = -c\ D_{AB}\ \frac{dy_A}{dr} + y_A\left(N_{A,r} + N_{B,r}\right)$$

The air outside of the water is taken as stagnant and non-diffusing so $N_{B,r} = 0$. Upon rearranging, we get to the form below.

$$N_{A,r} = \ -\frac{c\ D_{AB}}{(1 - y_A)}\ \frac{dy_A}{dr}$$

The molar flux depends on r since the area changes with time, but using a quasi-steady state assumption the mass transfer rate, $4\pi r^2\ N_{A,r} = W_A$ is taken to be independent of r and constant.

$$W_A = 4\pi r^2\ N_{A,r} = \ -4\pi r^2\ \frac{c\ D_{AB}}{(1 - y_A)}\ \frac{dy_A}{dr}$$

The above expression is integrated from r_1 to r_2, set at an infinite distance, after separating variables.

$$W_A \int_{r_1}^{r_2} \frac{dr}{r^2} = -4\pi\ c\ D_{AB}\ \int_{y_{A1}}^{y_{A2}} \frac{dy_A}{(1 - y_A)}$$

The result of the integration is:

$$W_A \left(\frac{1}{r_1} - \frac{1}{r_2}\right) = -4\pi\ c\ D_{AB}\ ln\left(\frac{1 - y_{A2}}{1 - y_{A1}}\right)$$

However; $r_2 \gg r_1$, so the above is further simplified to:

$$\frac{W_A}{r_1} = -4\pi\ c\ D_{AB}\ ln\left(\frac{1 - y_{A2}}{1 - y_{A1}}\right)$$

After multiplying by r_1, the expression for W_A is given as:

$$W_A = -4\pi\ r_1\ c\ D_{AB}\ ln\left(\frac{1 - y_{A2}}{1 - y_{A1}}\right)$$

A mass balance is set up around the sphere using the right side of the above equation, after multiplying it by the molecular mass, M.

$$\frac{d}{dt}\left(\frac{4}{3}\pi\, {r_1}^3\, \rho_A\right) = -4\pi\, M\, r_1\, c\, D_{AB}\, ln\left(\frac{1-y_{A2}}{1-y_{A1}}\right)$$

$$4\pi\, {r_1}^2\, \rho_A \frac{dr_1}{dt} = -4\pi\, M\, r_1\, c\, D_{AB}\, ln\left(\frac{1-y_{A2}}{1-y_{A1}}\right)$$

$$r_1\, dr = -\, Mc \frac{D_{AB}}{\rho_A}\, ln\left(\frac{1-y_{A2}}{1-y_{A1}}\right) dt$$

The right side of the above equation remains constant with respect to time, all of it is set as K:

$$r_1\, dr = -Kdt$$

The variable r_1 is changed to r and then to find the time it takes for the sphere to completely disappear the above is integrated as follows:

$$\int_{r_0}^{0} r\, dr = -K \int_0^t dt$$

This gives the time required for the sphere to go from an initial radius of r_0 until it completely disappears. The final relation is:

$$t = \frac{{r_0}^2}{2K}$$

The time that it takes for a droplet to evaporate is a function of the radius squared. The data collected of deforming radii versus time follows this relation. Below is a plot of the stretch ratio squared versus time, for a typical droplet. It shows the deformation up until the point of creasing.

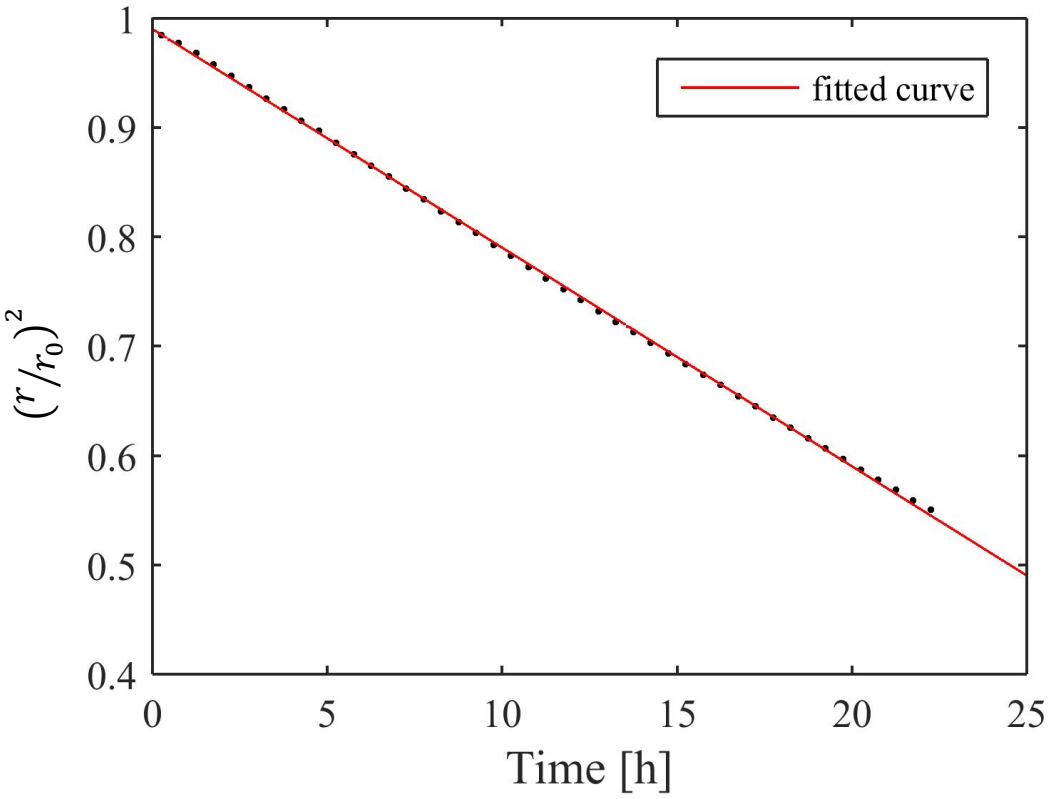

Fig. 3.9: The phenomenon observed in droplet deformation (black dots), with measurements taken every 30 minutes, fits the theoretical prediction that the process is evaporation. Evaporation predicts that there is a linear relationship between time and the radius squared.

3.5. Pressure at Creasing

The pressure attained at the point of creasing for all samples is shown, after creasing the method of using the stretch ratio to calculate the pressure fails because the droplets are no longer spherical. The pressures that are attained are well below most reported values of the cavitation pressure of water, which is at least -20 MPa [16][17].

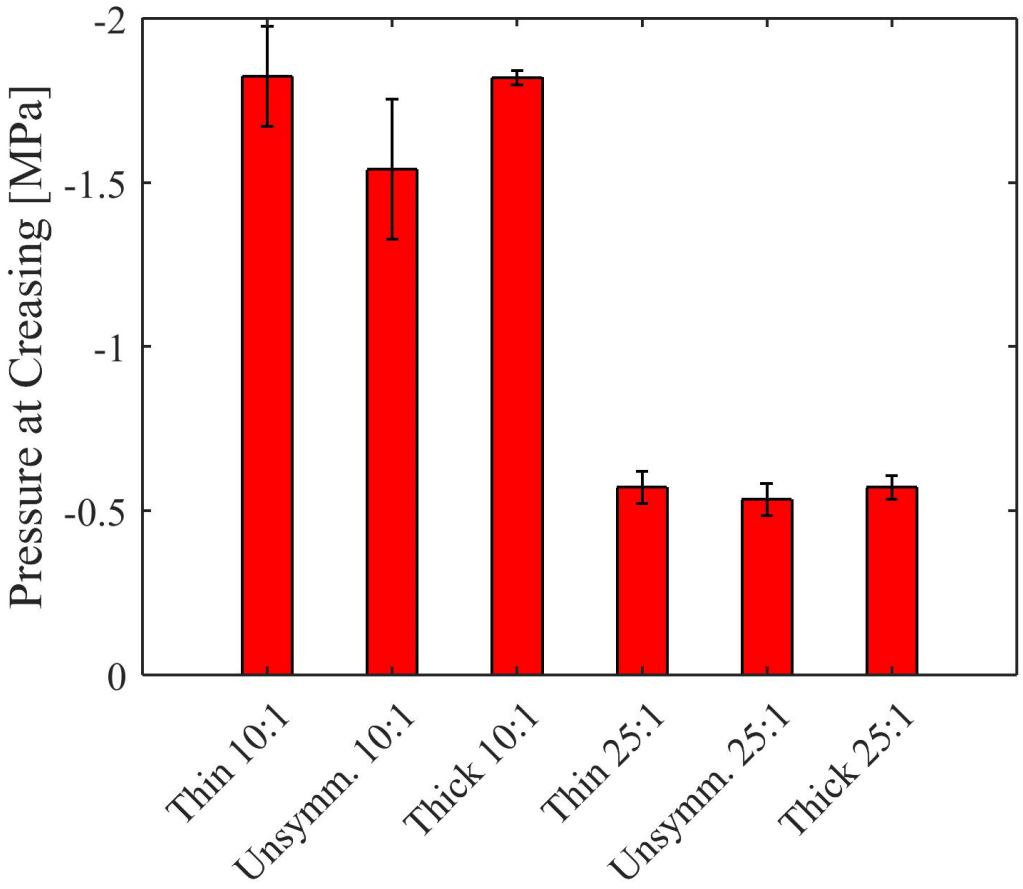

Fig. 3.10: The pressure achieved at creasing in all samples is well below reported cavitation pressures of water of -20 to -30 MPa. Droplets usually do not cavitate until after creasing, where the pressure would be expected to be closer to the cavitation pressure. Pressure in droplets cannot be measured once creasing occurs.

The tension reported uses a Neo-Hookean model to calculate the pressure from the stretch ratio. This equation is given by [10]:

$$P = E\left(\frac{5}{6} - \frac{2}{3}\lambda^{-1} - \frac{1}{6}\lambda^{-4}\right)$$

Where λ is the stretch ratio r/r_0. A term for surface tension is neglected from this equation because for the length scales of the droplets, the term is miniscule. The elastocapillary length was shown to play a larger role in the 25:1 PDMS, but even this length was still 10,000 times smaller than the radius of the droplets. Therefore, the surface energy term can be neglected. The Neo-Hookean model does not account for any strain hardening; therefore, these reported pressures are likely below the actual pressure in the droplet. The tension in the 10:1 samples is higher than in the 25:1 samples at the point of creasing due to the dependence of pressure on Young's Modulus and this value being higher in the 10:1 samples. A stiffer sample reaches a higher tension that a less stiff sample if they both reach the same stretch ratio. Cavitation occurred before creasing in only thick samples and never in thin samples. This could be due to the ability of droplets within thin samples to pull on the nearest free boundary, sucking it inwards. Perhaps by pulling in this surface it prevents cavitation from occurring by prevent the tension from increasing as drastically in thick samples. Alternatively, the particular shape that the droplets take on could prevent irregularities on the inner surface from nucleating cavitation.

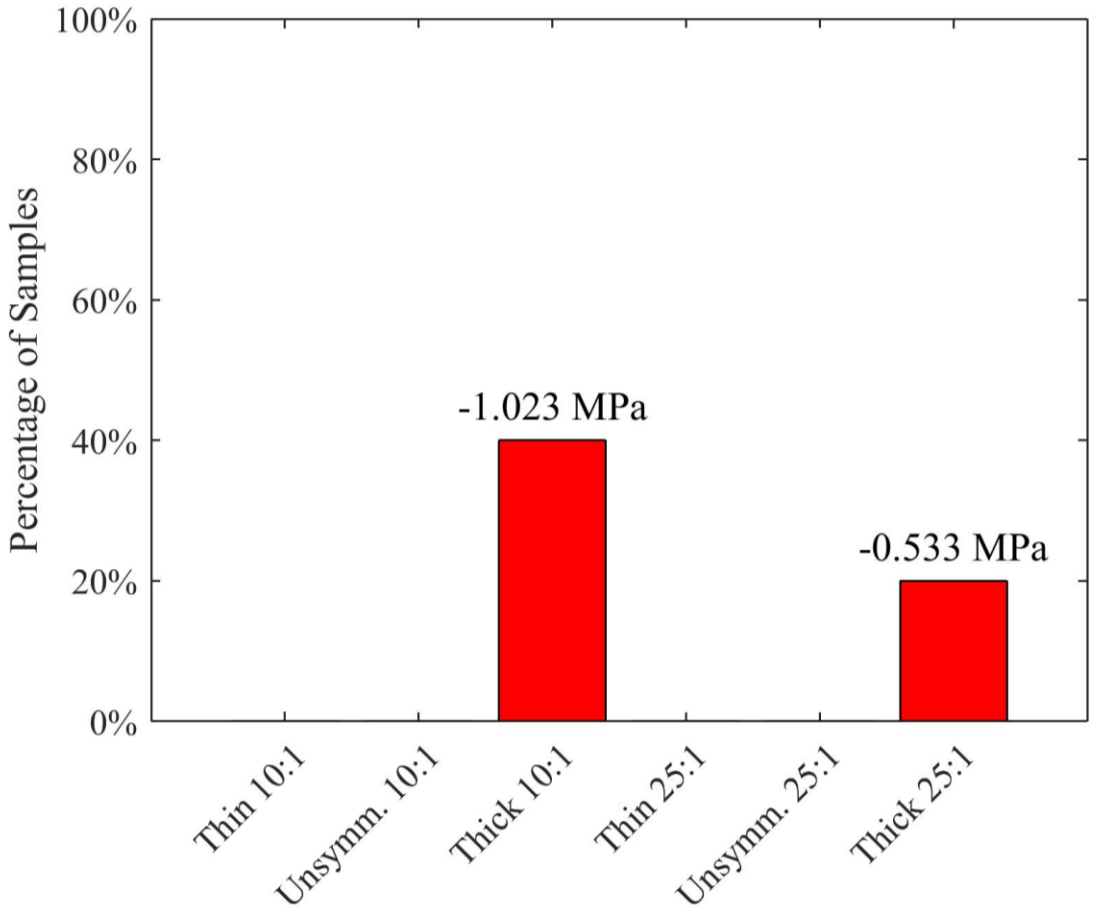

Fig. 3.11: Droplets in 10:1 thick samples fail to reach creasing 40% of the time while 20% of the droplets in 25:1 thick samples fail to reach creasing. All droplets of other types reach creasing. Since this happens in both soft and hard elastomers with thick boundary conditions, there could be some reason that thick boundary conditions cause this behavior. The average pressures at which the droplets cavitated is shown above each bar. This pressure is much below the cavitation pressure of water.

3.6. Cavitation

Cavitation is the formation of a vapor phase within a liquid, when a liquid experiences a reduction in pressure. As water evaporates out of the droplet it reduces in size and a tension builds in the droplet. The potential of the droplet to deform the surrounding elastomer is based on the amount of tension that can be held in the water. In order for a vapor to form in a liquid it must nucleate [18]. As soon as a sufficiently large nucleus of vapor forms within a droplet, cavitation occurs. The cavity grows and a large vapor-liquid surface is formed within the embedded droplet. The surface tension of the vapor is unable to hold the deformed droplet and the solid returns to its undeformed shape.

Water is able to withstand a tensile stress, until that stress reaches a level that causes cavitation. The ability of water to maintain tensile stress allows it to be pulled through roots and up trees, thus allowing tall trees to survive. Wheeler and Stroock measured the probability of cavitation of water that had reached equilibrium as a function of multiple vapor pressures. There is a dramatic transition in the probability of cavitation when the tension of the water is -22.15 ±0.72 MPa [16]. However, another source reported a study of cavitation using two methods to verify their results and reported cavitation pressures of -26 MPa at 0 °C and -17 MPa at 80 °C [17]. Both of these sources seem to confirm that the cavitation pressure should be around -20 MPa, when considering elevated temperatures. An important caveat is that these experiments are able to achieve such high negative pressures only because of pristine water purity. It has been reported that a critical negative pressure of -140 MPa had been observed in ultrapure water, at 42 °C [19]; however, this is measured in liquid inclusions inside of minerals, such as quartz. That situation is much different from the present study since droplets are embedded in elastomers. Water purity alone is not the sole cause for cavitation; surface roughness can provide sites for

nucleation of a gas bubble that triggers cavitation. Trapped gases in the water can nucleate at low negative pressures, around -4 MPa [17]. Because of sites such as this, the realistic cavitation limit of the water is greatly reduced. Gas bubbles are observed on the inner surfaces of droplets and could be a contributing factor as to why some droplets cavitate before creasing.

The tension in the liquid increases as the droplet shrinks, this causes dissolved gasses to come out of solution and collect on the inner surface. Fig. 3.12 shows images of gases collecting on the surface. The gases collect on the surface of the PDMS, unable to permeate. Since the tension on the water is at a higher magnitude throughout breathing in the 10:1 samples, more gas bubbles appear on the surface of these droplets. From Fig. 3.11 it can be seen that more droplets in the 10:1 elastomer cavitate early than in the 25:1, this could be due to the larger presence of gas bubbles forming on the inner surface of the droplet.

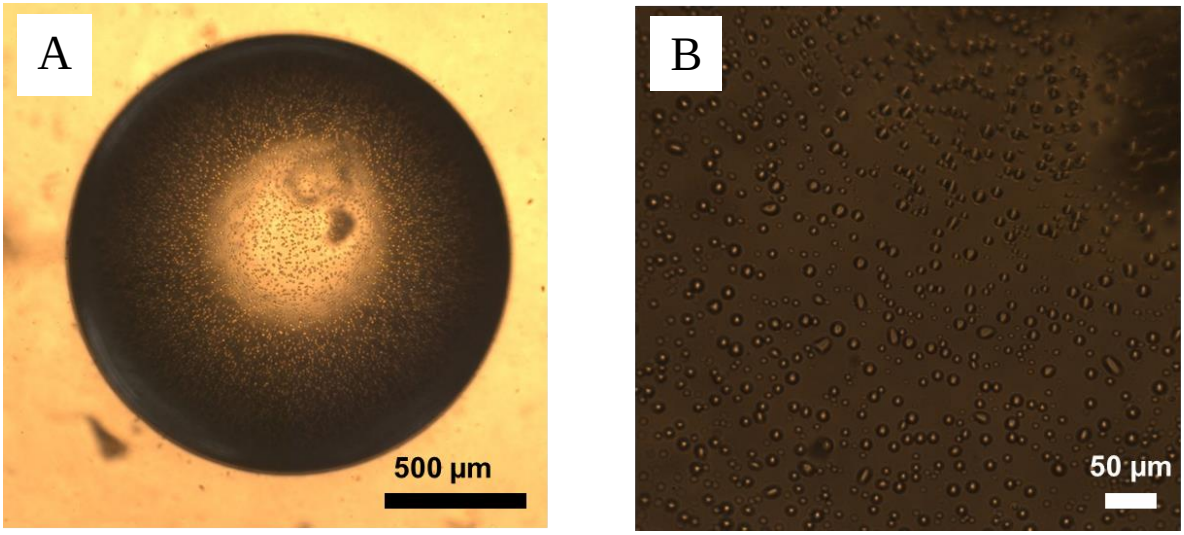

Fig. 3.12: (A) A droplet has reached a pressure where gas bubbles begin to nucleate on the inside surface. (B) Closer inspection of the gas bubbles.

Chapter 4: Self-Actuation of a Soft Solid-Liquid Composite

The goal is to use what has been learned by studying the deformation of water droplets inside of elastomers to guide the development in producing self-actuatable, soft, solid-liquid composites that mimic the behavior of the leptosporanguim spore-launching catapult.

4.1. Fabrication Difficulties

There were two different ways to approach the issue of fabrication. The choices were either to create the soft matrix first or to place the water droplets first. It may seem counterintuitive to place the water droplets first, but since PDMS starts as liquid this is possible, and turns out to be the most feasible way to produce replicas. By injecting water droplets into the liquid PDMS and then quickly curing the PDMS around them, it is possible to set the droplets completely inside the PDMS. Droplets will still shift, but the boundaries of the sample can be trimmed to an appropriate size. From Fig. 4.1 we can see that the actual leptosporangium has one side that is thick (the annulus) and another side that is thin to allow water to evaporate and collapse that side. This can be achieved by placing or trimming the replica so that the droplets are arranged near the edge of the same boundary.

4.2. Free Boundary Pulled In

Over the course of examining the creasing behavior of droplets (Chapter 3), those droplets that were too close to the edge of the sample pulled in the outside face of the sample. This behavior can be observed in Fig. 4.2, where the droplet draws the edge in to a point.

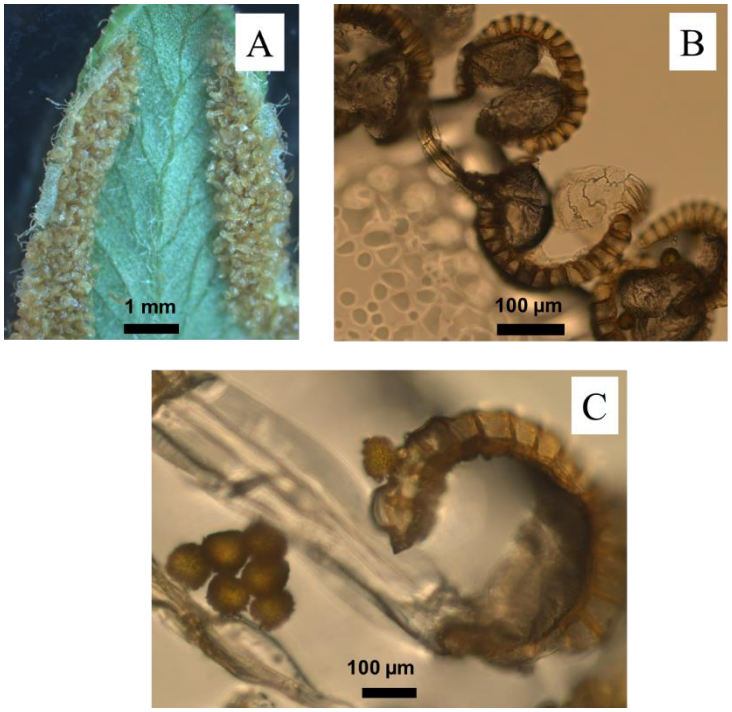

Fig. 4.1: (A) A fern frond, showing collections of many leptosporangium. (B) Empty leptosporangium catapults. (C) A leptosporangium with spores.

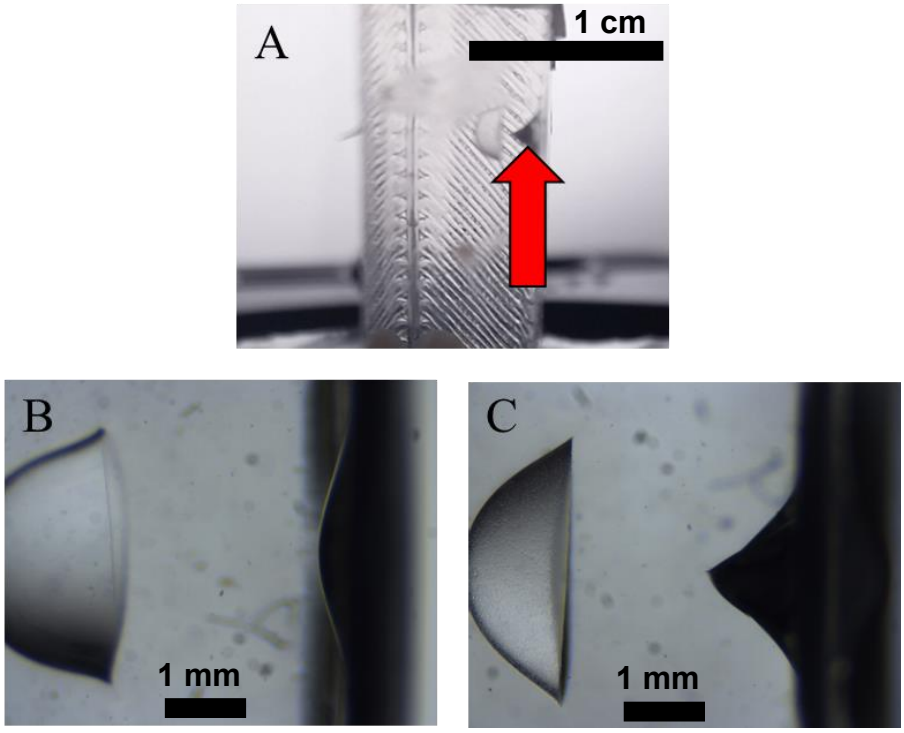

Fig. 4.2: (A) A droplet near the boundary, sucking in the free boundary. This can be observed with the naked eye. Another droplet that begins to deform the free boundary (B) and then at a later time (C) the deformation has increased.

Droplets that were within about one radius of the boundary had this same effect every time, so this behavior was used to mimic the leptosporangium. If multiple droplets, all in a row, each pulled on the same free surface causing this creasing behavior, together they should be able to collapse one side and deflect the entire body.

4.3. Self-Actuation of Soft-Solid Liquid Composite

Using evaporation, multiple water droplets embedded within soft elastomeric material are able to move the entire solid. Multiple water droplets were placed in a row within PDMS and then one side of the PDMS was trimmed so that the edge was much less than one radius from the droplets. These water droplets evaporated and pulled in the nearest boundary, causing the entire "beam" of PDMS to bend. The results of this test are shown in Fig. 4.3. The entire replica can be thought of as a cantilevered beam that hangs straight down and then a point force at the bottom causes it to deflect. This beam can be thought of as a three-layered composite: a thin strip of PDMS, a porous middle layer containing water droplets, and a thicker strip of PDMS on the other side of the middle layer. Since only two droplets are completely visible, approximations based on this are made to estimate the amount of energy and strain energy density. Under these

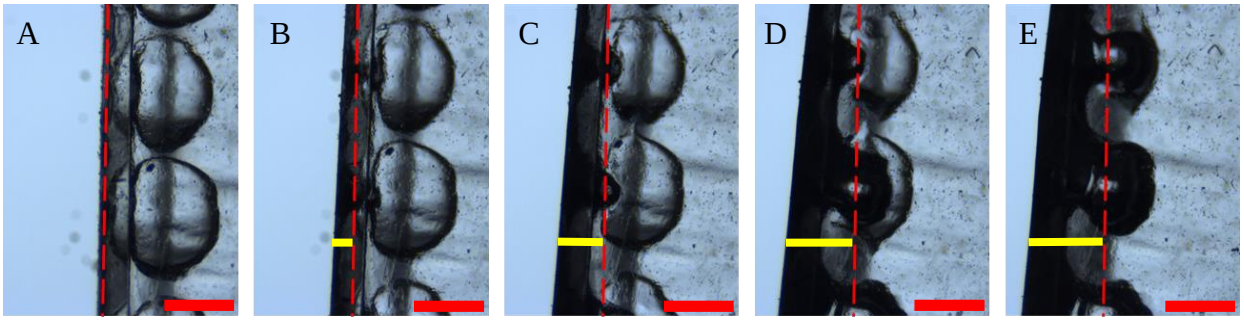

Fig. 4.3: A sequence of a replica over the course of deflection. The yellow bars show deflection from original position: A) 0 mm B) 0.264 mm C) 0.692 mm D) 1.065 mm E) 1.165 mm. Each image is 4 hours apart. The edge of the replica can be seen, specifically in "C" and "D," as it is pulled into the droplet, similar to Fig. 4.2. Droplets dry from the bottom first because the heat source is at the bottom. Red scale bar = 1 mm.

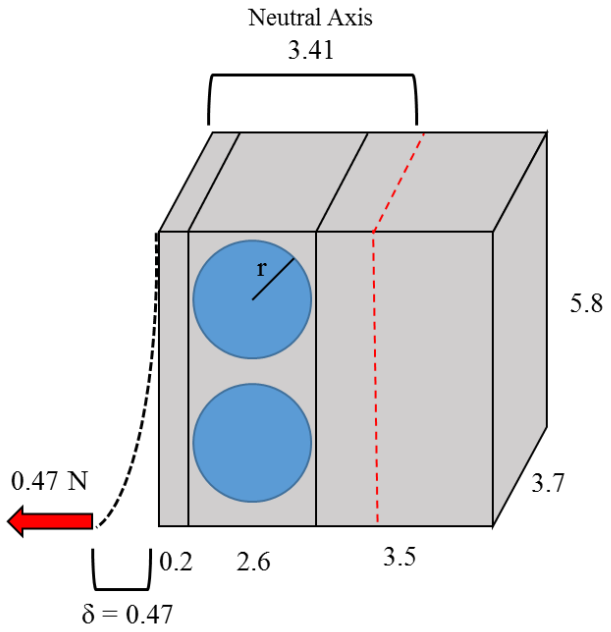

Fig. 4.4: A schematic showing the dimensions (all units are mm) of the composite beam approximation for the leptosporangium replica. This composite has three layers, the middle layer (with water droplets) has a porosity of 33%, resulting from droplets with radius, r = 1.3 mm. The neutral axis is 3.41 mm from the left, outer edge of the composite. The deflection, δ = 0.47 mm, caused by deforming droplets, is equivalent to a point load applied at the bottom of the beam of 0.47 N.

assumptions, the composite beam is assumed to be 5.8 mm long and deflect 0.47 mm, these values are measured and estimated from images in Fig. 4.3 and a schematic is shown in Fig. 4.4. The deflections shown in Fig. 4.3 account for the entire length of the replica, about 1.5 cm; however, the defection of 0.47 mm is estimated from the slope of the sample's edge at maximum deflection for a beam of 5.8 mm in length. The replica is constructed of 25:1 PDMS, with a Young's Modulus of 1 MPa, after taking into account the porosity of the middle layer and using equivalent area to determine the moment of inertia, an equivalent modulus of 0.67 MPa is used for each layer. Given the measured displacement, δ, we solve for a point load, F, that is assumed to be at the end of the beam, using the following equation.

$$F = {}^{3EI\delta}/_{l^3}$$

In this equation E is Young's Modulus, I is the moment of inertia, and l is the length of the beam. This results in a force, F, of 0.47 N being applied as a point lod. The strain energy is given by:

$$U = {F^2\ l^3}/{6EI}$$

where, the strain energy, U, is determined to be 1.1×10^{-4} J. This results in a conservative estimate for the strain energy density of about 0.8 J/kg. From Chapter 1, the *I. capensis* had 124 J/kg and *C. parviflora* had 89 J/kg, so this replica is not as efficient, but still performs relatively well given its simplicity. There were no reported values of strain energy density for *Polypodium aureum* or any other leptosporangiate ferns. This replica can be improved in design to increase the energy density. Like the leptosporangium, a stiff annulus-like portion should be added to the thick side of the replica and this thickness should be reduced. Reducing the thickness while maintaining a stiff spine, should result in more pronounced bending when the water droplets olapse. Furthermore, the size of the droplets can be increased, keeping all else the same to increase the distance that they are able to deform. To ensure that the droplets in the replica cavitate they will need to be moved further away from the nearest boundary so that they do not pull in the entire side as the water evaporates and then adhere the surfaces together, as can be seen in "E" of Fig. 4.3.

Chapter 5: Conclusions

Water droplets embedded within soft elastomeric materials are able to deform the elastomer as the water evaporates, because of surface energy and stiffness they will take on different configurations. Spherical droplets begin deformation by breathing, which is shrinking in a volume while remaining spherical. After breathing, droplets crease. Stiff elastomers remain spherical until a greater stretch ratio than those that are less stiff. Although surface energy is expected to have the opposite effect, at this length scale, which is much larger than the elastocapillary length, the stiffness of the modulus plays the dominant role when creasing sets in. However, once creasing does set in, surface energy appears to play a role in the way that channeling occurs in droplets. Lower surface energy enables deep channels to occur in droplets within stiffer elastomers. Up until the point of creasing, the pressure in droplets can be estimated by using the stretch ratio. This pressure is at least ten times below the reported cavitation pressure of water, so most droplets are able to continue to deform through creasing, resulting from the tension in water. Some droplets, however, cavitate before creasing. This can happen at points well below the expected cavitation pressure of water. This is most likely caused by surface irregularities that enable gasses to nucleate, providing areas that initiate cavitation. Droplets that deform near free boundaries are able to pull in those boundaries; this effect has been used to replicate movements achieved in the same manner as the leptosporangium [9]. Multiple droplets, aligned near a boundary, can work in concert to pull in the edge along the length of the small elastomeric beam. This causes deflection achieved by internal forces that are driven by environmental processes. This demonstrates a form of a self-actuated, soft, solid-liquid composite and although it is not as efficient as some plants, the design can be improved to enable it to perform closer to those levels.

5.1. Future Work: Characterizing Creasing, Pressure, and Self-Actuation

There are several areas that deserve further study, including: the effects of modulus and surface energy on creasing, pressure calculations for shrinking droplets, and furthering self-actuation. In droplets that are much larger than the elastocapillary length there seems to be a dominating presence from the stiffness of the material on when creasing sets begins. This should be studied across a wider range of stiffness, while altering surface energy to determine which factors are causing the results that we see. Alternatively, this same procedure should be done, but with much smaller droplets that are much closer in size to the elastocapillary length to see if the results from surface energy expectations do hold true. It appears that strain hardening effects the calculation of pressure. Instead of a neo-Hookean relation, a model that incorporates strain hardening could more accurately predict pressure within droplets given a certain stretch. Equilibrium experiments that will set a certain vapor pressure to a certain stretch ratio can help in determining the effects of strain hardening. Finally, the self-actuated composite should continue to develop, perfecting droplet placement and adding a stiff annulus to the replica. Cavitation has not yet been observed in replicas, which would be expected to return the deflection back to zero. Additionally, instead of straight replicas, curved replicas should be made to mimic the leptosporangium more accurately.

REFERENCES

[1] "Why Plants Need Water," *Clemson University Cooperative Extension*. [Online]. Available: http://www.clemson.edu/extension/horticulture/nursery/irrigation/why_plants_need_water.html. [Accessed: 20-Apr-2016].

[2] U. Zimmermann, F. Meinzer, and F.-W. Bentrup, "How Does Water Ascend in Tall Trees and Other Vascular Plants," *Annals of Botany*, vol. 76. pp. 545–551, 1995.

[3] D. Evangelista, S. Hotton, and J. Dumais, "The mechanics of explosive dispersal and self-burial in the seeds of the filaree, Erodium cicutarium (Geraniaceae).," *J. Exp. Biol.*, 2011.

[4] K. C. Vaughn, A. J. Bowling, and K. J. Ruel, "The mechanism for explosive seed dispersal in Cardamine hirsuta (Brassicaceae)," *Am. J. Bot.*, vol. 98, no. 8, pp. 1276–1285, 2011.

[5] M. Hayashi, K. L. Feilich, and D. J. Ellerby, "The mechanics of explosive seed dispersal in orange jewelweed (Impatiens capensis)," *J. Exp. Bot.*, 2009.

[6] R. D. Deegan, "Finessing the fracture energy barrier in ballistic seed dispersal," *Proceedings of the National Academy of Sciences*. 2012.

[7] D. L. Whitaker, L. A. Webster, and J. Edwards, "The biomechanics of Cornus canadensis stamens are ideal for catapulting pollen vertically," *Funct. Ecol.*, 2007.

[8] J. Edwards, D. Whitaker, S. Klionsky, and M. J. Laskowski, "Botany: a record-breaking pollen catapult.," *Nature*, 2005.

[9] X. Noblin, N. O. Rojas, J. Westbrook, C. Llorens, M. Argentina, and J. Dumais, "The Fern Sporangium: A Unique Catapult," *Science (80-.).*, vol. 335, pp. 1322–1322, 2012.

[10] S. Cai, K. Bertoldi, H. Wang, and Z. Suo, "Osmotic collapse of a void in an elastomer:

breathing, buckling and creasing," *Soft Matter*, vol. 6, no. 22, p. 5770, 2010.

[11] D. Chen, S. Cai, Z. Suo, and R. C. Hayward, "Surface Energy as a Barrier to Creasing of Elastomer Films: An Elastic Analogy to Classical Nucleation."

[12] Z. Wang, A. A. Volinsky, and N. D. Gallant, "Crosslinking effect on polydimethylsiloxane elastic modulus measured by custom-built compression instrument," *J. Appl. Polym. Sci.*, vol. 41050, pp. 1–4, 2014.

[13] Z. Suo, "Elastocapillarity," *iMechanica*, 2013. [Online]. Available: http://imechanica.org/files/Elastocapillarity 2013 02 03.pdf. [Accessed: 20-Apr-2016].

[14] V. Trujillo, J. Kim, and R. C. Hayward, "Creasing instability of surface-attached hydrogels," *Soft Matter*, vol. 4, no. 3, p. 564, 2008.

[15] T. K. Nguyen, "No Title." [Online]. Available: https://www.cpp.edu/~tknguyen/che313/pdf/chap1-3.pdf. [Accessed: 10-Apr-2016].

[16] T. D. Wheeler and A. D. Stroock, "The transpiration of water at negative pressures in a synthetic tree," vol. 455, no. September, 2008.

[17] F. Caupin and E. Herbert, "Cavitation in water: a review," *Comptes Rendus Phys.*, vol. 7, no. 9–10, pp. 1000–1017, 2006.

[18] P. Eisenberg, *Cavitation*. Hydronautics, Incorporated, 1968.

[19] Q. Zheng, D. J. Durben, G. H. Wolf, and C. A. Angell, "Liquids at large negative pressures: water at the homogeneous nucleation limit.," *Science*, vol. 254, no. 5033, pp. 829–32, 1991.

[20] M. Hayashi, S. P. Gerry, and D. J. Ellerby, "The seed dispersal catapult of Cardamine parviflora (Brassicaceae) is efficient but unreliable," *Am. J. Bot.*, 2010.